

## Characterization of a *Schistosoma mansoni* NDPK expressed in sexual and digestive organs

Juliana Roberta Torini<sup>1†</sup>, Adriano de Freitas Fernandes<sup>1†</sup>, Vitor Hugo Balasco Serrão<sup>1,2†\*</sup>, Larissa Romanello<sup>1</sup>, Louise E Bird<sup>3</sup>, Joanne E Nettleship<sup>3</sup>, Raymond J Owens<sup>3</sup>, José Brandão-Neto<sup>4</sup>, Ana Eliza Zeraik<sup>1</sup>, Ricardo DeMarco<sup>1</sup>, Humberto D'Muniz Pereira<sup>1</sup>.

1- Laboratório de Biologia Estrutural, Instituto de Física de São Carlos, Universidade de São Paulo, 13563-120, São Carlos, SP, Brazil. 2-Department of Medicine Pathobiology, University of Toronto, M5S 1A8, Toronto, Canada. 4- OPPE-UK, Research Complex at Harwell, Rutherford Appleton Laboratory, Oxford, OX11 0FA, UK. 5-Diamond Light Source, Harwell Science and Innovation Campus, Didcot, Oxfordshire, OX11 0DE, UK.

<sup>†</sup> The authors contribute equality to this work.

\*To whom correspondence should be addressed: Dr. Vitor Hugo Balasco Serrão, Department of Medicine Pathobiology, University of Toronto, 1 King's College Circle, M5S 1A8. Toronto, ON, Canada, Telephone (+1) 647-996-3914; e-mail: vitor.serrao@utoronto.ca

Keywords: Crystallography; Isothermal Titration Calorimetry; NDPK, *Schistosoma mansoni*

This work was supported by Grants 2012/14223-9 (HMP), 2012/10213-9 (JRT) 2012/23730-1 (VHBS) from São Paulo Research Foundation (FAPESP) and CNPq 474402/2013-4 (HMP); 134013/2015-8 (AFF), 140636/2013-7 (VHBS) and MR/K018779/1 (LEB, JEN, RJO). Also, we would like to thank CAPES.

## Abstract

Nucleoside diphosphate kinases (NDPKs) are crucial to keep the high triphosphate nucleotide levels in the biological process. The enzymatic mechanism has been extensively described; however, the structural characteristics and kinetic parameters have never been fully determined. In *Schistosoma mansoni*, NDPK (*Sm*NDPK) is directly involved in the pyrimidine and purine salvage pathways, being essential for nucleotide metabolism. The *Sm*NDPK enzymatic activity is the highest of the known purine metabolisms when compared to the mammalian NDPKs, suggesting the importance of this enzyme in the worm metabolism. Here, we report the recombinant expression of *Sm*NDPK that resulted in 1.7 and 1.9 Å apo-form structure in different space-groups, as well as the 2.1 Å *Sm*NDPK.ADP complex. The binding and kinetic assays reveal the ATP-dependence for enzyme activation. Moreover, *in situ* hybridization showed that *Sm*NDPK transcripts are found in reproductive organs and in the esophagus gland of adult worms, which can be intrinsically related with the oviposition and digestive processes. These results will help us fully understand the crucial participation of this enzyme in *Schistosoma mansoni* and its importance for the pathology of the disease.

## 2- Introduction

Nucleoside diphosphate kinase (EC2.7.4.6) is the enzyme responsible for the reversible transference of  $\gamma$ -phosphoryl group from a triphosphate to a diphosphate nucleoside [1, 2]. This transfer mechanism occurs through an enzymatic transitory state, where a catalytic histidine is temporarily phosphorylated, creating a “*ping-pong*” mechanism [3], as can be seen at schema below:



The NDPK is found in all cells and it is able to use both purines and pyrimidines nucleotides, as well as oxy and deoxy derivatives, showing low specificity to bases moiety of the nucleotides [4, 5]. These characteristics confer an important role on the balance and maintenance of oxy- and deoxy triphosphate nucleoside into cells [6-8] and could be related with cardiovascular disease [9] and problems during the metastasis processes [10].

Due to their importance in cell metabolism, many structural studies have been performed (154 PDB entries). Interestingly, in only a few the native substrates (ADP, ATP, CDP, CTP, GDP, dGTP/GTP, TDP, and UDP) were used.

The *S. mansoni* parasite is an atypical trematode (the adult stage is sexually dimorphic); it is the causative agent of schistosomiasis, a neglected tropical disease that, according to World Health Organization, affects 218 million of people worldwide [11]. *S. mansoni* is incapable of synthesizing purine nucleotides or their immediate precursors by the *de novo* pathway [12-20], thus the purine salvage pathway represents a vital pathway for the maintenance of ATP or GTP energy systems, with NDPK occupying a central position in the control of cell functions.

This enzyme is important in several biological processes from bacteria to humans. In the *Schistosoma mansoni* parasite, NDPK activity is the highest of the purine metabolism in adult schistosomes crude extracts, and when compared with mammalian tissues, is 5 to 10 fold greater in *S. mansoni* [16], indicating that NDPK activity is even more pronounced in the parasite metabolism.

Here, we describe the three-dimensional structure of NDPK from *Schistosoma mansoni* (SmNDPK) obtained by protein crystallography. In addition, nucleotide binding assays using a non-hydrolysable phosphate donor were conducted by

Isothermal Titration Calorimetry, showing the sequential binding preference. Finally, we show the localization of *SmNDPK* transcripts in the gonads and anterior esophagus of adult worms by whole-mount *in situ* hybridization (WISH). Therefore, it is possible to hypothesize that *SmNDPK* is particularly important to parasite reproduction and digestion. The predominant localization in the ovaries of female adult worms makes this protein likely to be involved in the oviposition process, which is a key pathology feature in the development and transmission of the disease [21].



### 3- Materials and Methods

#### *Cloning, Expression, and purification of recombinant SmNDPK*

The *SmNDPK*(*Smp\_092750*) gene was synthesized with codon optimization by GenScript company and cloned into pOPINF[22] using the *In-Fusion* method (Clontech, Mountain View, CA, United States). pOPINF-*Smndpk* vector was transformed into Omni-MaxII cells (Invitrogen), transformants were selected using the chromogenic substrate X-Gal and by colony PCR, white colonies were picked and grown in Power Broth™ medium supplemented with 50 µg/mL of carbenicillin antibiotic at 37 °C and 600 rpm for 16 hours. The plasmid mini-preps were performed on the *Onyx* robotic system according to the manufacturer's protocols. The purified plasmid (pOPINF-*Smndpk*) was used in the transformation of *Escherichia coli* Rosetta2™ (DE3) strain. The protein was expressed using Power Broth™ medium supplemented with 50 µg/mL of carbenicillin and 35 µg/mL chloramphenicol. The cells were incubated at 37 °C for 4 hours to OD<sub>600</sub> of about 0.5 and induced with 0.1 mM of isopropyl β-D-1-thiogalactopyranoside (IPTG), then were incubated at 18 °C for 16 hours with continuous shaking at 250 rpm, harvested by centrifugation at 5000g for 15 minutes and frozen at -20 °C.

The cells were defrosted and lysed in a different lysis buffer (50 mM potassium phosphate pH 7.6, 300 mM NaCl, 10 mM imidazole, 5 mM 2-mercaptoethanol, 0.1 mM dithiothreitol (DTT) and 1 mM phenylmethylsulphonyl fluoride (PMSF). The cells were lysed by sonication followed by centrifugation (4700 g for 40 min. at 4 °C). The clarified lysate was applied to Co<sup>2+</sup>-agarose column (Qiagen), after column wash, the 6His-*SmNDPK* was step-eluted with elution buffer (50 mM potassium phosphate pH 7.6, 300 mM NaCl, 200 mM imidazole and 5 mM 2-mercaptoethanol).

The 6-His-Tag was cleaved by addition of 3C protease (1 U/100 µg fusion protein) with overnight incubation at 4 °C. Cleaved *SmNDPK* was purified from the digest using a reverse purification in Ni<sup>2+</sup>-NTA column. The eluate was then concentrated and followed by dialysis in appropriate buffer to further studies. All steps from expression were analyzed by SDS-PAGE 15%.

### ***Binding and Kinetic Assays by Isothermal Titration Calorimetry***

The *Sm*NDPK binding assays during the nucleotides recognition were performed by isothermal titration calorimetry (ITC) experiments with titration in a VP-ITC calorimeter [23]. The apparent molar enthalpy ( $\Delta H_{app}$ ) from each interaction was monitored by sequential titrations from the triphosphate nucleotides (ATP, CTP, GTP, TTP, UTP and non-hydrolysable nucleotide - ATP $\gamma$ S) as recognized as substrates for NDPKs.

*Sm*NDPK was prepared in phosphate buffer (50 mM potassium phosphate pH 7.6, 150 mM NaCl, 1 mM MgCl<sub>2</sub>) and 100  $\mu$ M were placed in the VP-ITC experimental cell. The nucleotides (Sigma-Aldrich) were prepared at 1 mM by dilution in the same buffer and titrated using multiple injections (2  $\mu$ L each) at 25 °C and monitored the heat exchange during 160 s. These substrates were titrated by 20-35 injections with a stirring speed of 300 rpm [24, 25]. The  $\Delta H_{app}$  was obtained by integration of the area under the peak yields after subtracting the heat of dilution from the nucleotides [24, 26].


For monitoring the diphosphate nucleotides binding, the same procedure was performed using the same experimental procedures. However, the results showed inexpressive binding results (no detectable heat exchange), revealing no binding to diphosphate nucleotides. Then, the diphosphate nucleotides binding assays were performed using 1 mM ATP $\gamma$ S as excess placed at cell and syringe during the titrations. The initial *Sm*NDPK.ATP $\gamma$ S complex was evaluated in order to understand the preference and capability to recognize and bind to the diphosphate nucleotides. The results were processed using the Origin 7.0 software associated to the microcalorimeter, and the integral of the curve obtained reflects the heat variation in the system using sequential binding site model ( $n = 6$ ) to perform the best fit considering that *Sm*NDPK is a hexamer in solution. All the results were determined by triplicate measurements. Binding using bovine serum albumin (BSA, Sigma-Aldrich A2153) was used as negative control being performed at the same experimental conditions.

In addition, the *Sm*NDPK enzymatic assay to determine the kinetics parameters of GDP phosphorylation by ATP consumption was also performed by ITC. In spite of NDPKs enzymes present a “*ping-pong*” reaction mechanism, the fast

reaction treatment from the single-injection assays may help to infer the kinetics parameters [26].

To measure the apparent molar enthalpy ( $\Delta H_{app}$ ), 2  $\mu$ M *Sm*NDPK was titrated with a fast injection (2.5 seconds) with 20  $\mu$ L ATP (1 mM), at 15 °C and the heat exchange was monitored for 1200 seconds. Enzyme and ATP were prepared in phosphate buffer (50 mM potassium phosphate pH 7.6, 150 mM NaCl, 1 mM  $MgCl_2$ ) containing 1 mM of GDP. After ATP heat dilution subtraction, it was possible to obtain the  $\Delta H_{app}$  by the integration of the area under the peak yields [24, 26].

The results were also processed using Origin 7.0 where the integral of the curve obtained reflects the heat variation in the system and the kinetic parameters were determined by the Michaelis-Menten model applied to single-peak analysis [27].

  
A crystallization screen (OPPF-UK) was performed (using *Sm*NDPK prepared in Tris buffer), to determinate the optimal concentration of sample for setting up the crystallization experiments. Using *Sm*NDPK at 5mg/mL, crystallization screening experiments were performed in OPF-UK on Cartesian 2 using screen solutions from Molecular Dimension (Morpheus® and JCSG-*plus*™), Hampton Research (Index HT™) and Jena Bioscience (JBScreen Wizard 1 and JBScreen Wizard 2) using sitting drop.

For co-crystallization experiments, the *Sm*NDPK was incubated with 5mM of each ligand (ADP, ATP, and GDP), and submitted to crystallization trials with 1:1  $\mu$ L drops in a Honeybee 961 robot in Greiner Crystal Quick plates and incubated at 18 °C. Different crystals forms appear after two days and reach their maximum size (~150 $\mu$ m).

The crystals were mounted in microloops, cooled with 20% glycerol or PEG200 and frozen in liquid nitrogen. Diffraction data were measured using synchrotron radiation at beamline I04-1 of the Diamond Light Source (DLS, Harwell, UK). The data were indexed, integrated and scaled using the Xia2 [28-31].

The *Sm*NDPK-apo enzyme structure was solved by molecular replacement using the Phaser program [32], employing NDPK enzyme from *Drosophila melanogaster* (PDB.ID:1NDL) which shares 62% identity as a search model. The remaining structures were also solved by molecular replacement, using as model one

of the structures previously refined. The refinement was carried out using Phenix[33] and the model building performed COOT [34], using a weighted 2Fo–Fc and Fo–Fc electron density maps. In all cases the behavior of R and  $R_{\text{free}}$  was used as the principal criterion for validating the refinement protocol and the stereochemical quality of the model was evaluated with Molprobity [35]. The coordinates and structure factors have been deposited with the PDB under the following codes: *Sm*NDPK-apo ( $C_2$ symmetry) – 5IOL, *Sm*NDPK-apo ( $P6_322$ symmetry) – 5IOM, and *Sm*NDPK.ADP complex – 5KK8.

### ***Whole-mount in situ hybridization (WISH)***

A fragment spanning 300 bp of *S. mansoni* NDPK was amplified from adult worm's cDNA, using the following primers: *Sm*NDPK\_Foward primer: 5'-ATGGAACGGACGTTTATTATGG-3' and *Sm*NDPK\_Reverse primer: 5'-TGATCCAGGACAACCTTGCTTC-3'. The amplicon was inserted into a pGEM-T Easy vector (Promega) and sequenced to confirm the amplicon identity as well as the orientation of the strands into the vector. Riboprobe kit (Promega) was used to produce sense or anti-sense Digoxigenin(DIG)-labelled RNA probes, following manufacturer's instructions. Whole-mount *in situ* hybridization (WISH) experiment was carried out as previously described [36, 37]. In brief, *S. mansoni* adult worms were fixed in Carnoy's fixative (ethanol:chloroform: glacial acetic acid in a 6:3:1 ratio) on ice for 2 h, followed by fixation in MEMFA (0.1 M MOPS pH 7.4, 2 mM EGTA, 1 mM  $MgSO_4$ , 3.7% formaldehyde) for 1 h and then washed and stored in 100% ethanol at -20 °C. The worms were permeabilized with proteinase K (Roche) after being rehydrated through a methanol series to PBS with 0.3% Triton-X 100 (PBSTx) and then were post-fixed in 4% paraformaldehyde (PFA). Hybridization was performed with 1  $\mu$ g/mL of antisense DIG-labelled RNA probe in hybridization buffer (50% formamide, 5 X SSC, 1% Tween-20 and 1 mg/mL of RNA from torula yeast) at 56 °C for 18-20 h. The control group was incubated with the DIG-RNA probe corresponding to the sense strand of *Sm*NDPK. The worms were then extensively washed and incubated in blocking solution (100 mM maleic acid, 150 mM NaCl, 0.1% Tween-20, pH 7.5 containing 10% horse serum) for 2 h at room temperature before the incubation with anti-DIG-alkaline phosphatase-conjugated antibody (Roche) diluted in blocking solution (1:2000), carried out at 4 °C for 16 h.

The signal was developed by nitro-blue tetrazolium chloride (NBT) and 5-Bromo-4-chloro-3'-indolylphosphate p-toluidine (BCIP) solutions (Roche). Specimens were imaged an Olympus BX53 microscope.

## 4- RESULTS AND DISCUSSIONS

### *SmNDPK sequence analysis and expression in adult worms*

A search on *S. mansoni* genome available on GeneDB[38] allowed the detection of five annotated NDPK genes. We selected one gene (*Smp\_092750*, which we named *SmNDPK*) coding for the *S. mansoni* NDPK displaying the highest identity with the previously described NDPKs from humans for further studies (~60% identity to both *HsNDPK-A* and *HsNDPK-B*, Fig. 1).

The expression levels of this gene, calculated from RNA-Seq libraries of different life cycle stages and available on GeneDB, reveal that the *SmNDPK* expression in adult worms are approximately 3-fold higher than that of cercariae and 24 h-cultured schistosomula and 9-fold higher than 3 h cultured schistosomula. The localization of *SmNDPK* transcripts in adult worms was determined by WISH experiments and showed strong labeling in the ovary and vitellaria of female adult worms (arrows in Fig 2A and B). Male adult worms displayed staining in the testes (arrow in Fig 2C). No staining was observed in the control group, incubated with *SmNDPK* sense riboprobe (Fig 2D). This reinforces the idea that the main function of this protein is associated with the mature sexual apparatus of adult worms, since inspection of data from a previously described RNA-Seq analysis from gonads of *S. mansoni* adult worms [39] reveals that *SmNDPK* is upregulated in ovaries of paired females in comparison with unpaired females. Apart from the strong labeling observed in the reproductive organs of adult worms, labeling in the anterior region of the esophagus was also detected (Fig 2C arrow head). This appears to confirm a previous proteomic analysis of worm vomitus [40] that suggested that *SmNDPK* was involved in parasite digestion of host blood.

The *SmNDPK* codes a protein with 149 amino acids with a molecular weight of about 17 kDa that was successfully expressed in a heterologous system using pOPINF vector and purified, yielding 12 mg per liter of culture medium. Retention times in an analytical size exclusion chromatography of the purified protein suggested a hexameric conformation in solution (~120 kDa, data not shown), which is a common feature of NDPKs.

### ***Binding and Kinetics Assays***

Parks and Agarwal described NDPK enzyme [3] displaying many different substrates, where the general reaction is via “*ping-pong*” mechanism, as follows:  $\text{XDP} + \text{YTP} \leftrightarrow \text{XTP} + \text{YDP}$  (X and Y each represent different nitrogenous base). NDPKs activities maintain an equilibrium between the concentrations of different nucleoside triphosphates [41].

The binding assays using Isothermal Titration Calorimetry (ITC) with several nucleotides (Fig 3A-E) showed higher affinity for ATP and GTP with dissociation constants of 3.1 and 3.3  $\mu\text{M}$ , respectively. The other nucleotides tested showed significantly higher dissociation constants (Table 1). The ATP $\gamma$ S nucleotide also presented a binding profile with dissociation constant of  $(7.25 \pm 0.42) \mu\text{M}$ . BSA was used as negative control (Fig. 3G-H).

These results correlate with the described high availability in blood of adenine and guanine nucleotides based on Human Metabolome Database, HMDB ( $> 1300$  and  $\sim 56 \mu\text{M}$ , respectively) when compared with CTP, and both non-quantified nucleotides: TTP and UTP. Although ambiguous, the nucleotides concentrations in the bloodstream can be discrepant and vary from 28 up to 11,000 nmol/L depending on the procedures and experimental analysis.

Moreover, the promiscuities for the  $\gamma$ -phosphate donor, possibly using ATP or GTP, is evident based on the dissociation constants obtained; these results agree with the first proposal that *Sm*NDPK could use both as a phosphate donor [3].

On the other hand, the same procedure was performed for monitoring the diphosphate nucleotides binding. However, the results suggest an insignificant binding (data not shown).

The same assay using protein samples in a solution with 1 mM ATP $\gamma$ S (non-hydrolyzed nucleotide) alone and sequentially adding the diphosphate nucleotides, revealed that *Sm*NDPK displays higher affinity for these dinucleotides when previously bound to a trinucleotide (Fig 4A-E). The experiment using ADP revealed an exothermal interaction, which possibly indicated the formation of a ternary complex *Sm*NDPK:ATP $\gamma$ S:ADP, with high affinity ( $K_D = 1.45 \pm 0.06 \mu\text{M}$ ), about 8 times smaller than the same experiment using other dinucleotides (Table 1). The enzymatic activity of *Sm*NDPK was characterized as an endothermic reaction with enthalpy exchange reaction of  $\Delta H_{\text{ATP/GDP}} = + 2.0 \text{ kcal/mol}$  by a single injection ITC

under saturating conditions (data not shown). Further characterization by fast reaction analysis based on the single injection peak shows the  $K_M = (36.3 \pm 1.6) \mu\text{M}$  and  $k_{\text{cat}} = (0.68 \pm 0.01) \text{ s}^{-1}$  to ATP consumption and GTP formation (Table 1) obtained by Michaelis-Menten fit.

ATP affinity is similar to the previously described affinity for *Streptomyces coelicolor* [42] and 1000 fold higher than the affinity observed for human NDPK [43]. This high affinity might be connected with necessity for ATP absorption directly from the blood, being driven to keep the worm nucleotide metabolism from the absorbed ATP.

However, the GTP affinity is 20-fold higher than any of the previous NDPKs described on BRENDA database.

### ***SmNDPK structure***

Three *SmNDPK* structures were obtained: Apo structures in  $C_2$ ;  $P_6_32_2$  space groups and *SmNDPK* ADP complex in  $P_6_32_2$  space group. The  $P_6_32_2$  structure has two molecules per asymmetric unit and the  $C_2$  structure in space group has twelve molecules per asymmetric unit, forming two full hexamers. The X-ray data were collected in beamline I04-1 of the Diamond Light Source (UK) and used to obtain three-dimensional structures with resolution ranging from 1.79 Å (*SmNDPK*-apo  $C_2$ ) to 2.1 Å (*SmNDPK*-ADP). The data collection and refinement statistics can be seen in Table 2.

The *SmNDPK*'s functional unit is a hexamer as observed in other eukaryotic species (Fig 5A) and can be viewed as the stacking of two trimers. The *SmNDPK* monomer is composed by an  $\alpha/\beta$  domains, a central beta sheet with four antiparallel beta-strand ( $\beta_2$ ,  $\beta_3$ ,  $\beta_1$  e  $\beta_4$ ) surrounded by eleven alpha helices (Fig 5B).

All  $\alpha$ -helices, and  $\beta$  sheets positions are conserved with exception of a helix arrangement between residues 108 to 112 in humans.

A comparison of the structure with different ligands resulted in a maximum RMSD between chain A from *SmNDPK*-apo  $P_6_32_2$  and chain L from *SmNDPK*-apo  $C_2$  structures (Root mean-square deviation, RMSD 0.227 Å). This indicates that the ligand does not induce significant structural changes. The overlap of monomers from the structures obtained showed that the side chain positions of residues are broadly conserved; conformational changes are noted mainly in the side chains of the F57,



E121, L129, Q134, Q138 and K140 residues. The monomer B from *Sm*NDPK-apo C2 shows the highest number of residues with conformational changes in their side chains, along with a slight loop deviation (between L53 and F58 residues) of 2.6 Å.

The RMSD of *Sm*NDPK relative to human NDPK-A (PDB.ID 2HVD) and NDPK-B (PDB.ID 1NUE) is 0.573 Å and 0.398 Å, respectively. The main difference between the structure from schistosome and human proteins happens between Q111-N115 residues (corresponding to D108-N112 in *S. mansoni* NDPK), where there is a small  $\alpha$ -helix that is not present in *Sm*NDPK.

### Active site analysis

Analysis of the crystal structure from *Sm*NDPK allowed the characterization of the active site due to the ADP presence; the residues involved in its binding are conserved. In Fig 6, residues that belong to the catalytic pocket and nucleotide binding are shown (Fig. 6A-C). However, the main residues, responsible for the catalytic activity of the enzyme are away from the binding cleft. These residues determine the sequence HGS (H115, G116, and S117), that is conserved in all existing NDPKs (Fig 6C).

These HGS residues form the catalytic pocket exposed to solvent; there are no residues from neighboring subunits involved in the nucleotide binding. The direct interaction with ADP molecule occurs between the ribose portion and K9, T91, V109 and N112 residues. However, four other residues (L52; F57; L61; R102) collaborate, thus, stabilizing the purine portion. The NDPKs have low specificity to the base portion of nucleotides; the base binding happens inside of a hydrophobic cleft of the active site and, therefore, displays weak interactions with the protein.

This weak interaction with the base justifies the relatively low specificity of *Sm*NDPKs to various nucleotides and deoxy nucleotides tested, similarly to what has been described for other NDPKs [8].

## 5- DISCUSSION

Besides the huge structural information, the catalytic mechanism of NDPKs occurs through a very complex, but well-determined sequence of events that are well described and studied [6, 8, 44]. As previously characterized, the NTP phosphate donor binds in the catalytic pocket, located on the surface of each subunit of the hexamer. The NTP concentration is the main factor to determine which donor will be bound (since there is abundant ATP concentration in the cells, it is the most used NTP by NDPKs). In the next step, the catalytic histidine (H115 in *Schistosoma mansoni* NDPK determined based on sequence alignment) is phosphorylated by transferring the phosphate- $\gamma$  group (phosphate group furthest from the base), resulting in an intermediate state of the enzyme with the presence of a phosphohistidine. The phosphate group stabilization to form the phosphohistidine is aided by the action of serine S117, which helps to accommodate the phosphate group in the space left by the presence of G116. The concentration increases of a different NDP than that which is bound to the catalytic site displaces the equilibrium and makes the nucleotide leave the active site for the entry of a receptor nucleotide. The receptor NDP receives the phosphate group bound to phosphohistidine and leaves the site as a new NTP. When the *Sm*NDPK-apo and ADP structures were compared by superposition, no significant structural changes in active site were observed.

The binding assays reveal an ATP/GTP preference during the first step formation (dissociation constants in  $(3.10 \pm 0.02) \mu\text{M}$  and  $(3.30 \pm 0.07) \mu\text{M}$ , respectively), which could be explained by the blood availability in comparison with others triphosphate nucleotides. In addition, the sequential interaction using non-hydrolyzed nucleotide, ATP $\gamma$ S, showed that it has no preference for the second nucleotide (all the  $K_D$  are about  $10 \mu\text{M}$ ), indicating that the ATP/GTP are the major phosphate donors during the metabolic reaction. These hypotheses indicate the nucleotides pull is kept by the *Sm*NDPK, being highly active to be responsible for the diphosphate nucleotides conversion to triphosphates by ATP/GTP, obtained by feeding, as the  $\gamma$ -phosphate donor.

The kinetics assays also showed the *Sm*NDPK activity in function of  $\gamma$ -phosphate transfer from ATP to GDP, forming GTP and ADP. The  $K_M$  and  $k_{cat}$  values  $(36.3 \pm 1.6) \mu\text{M}$  and  $(0.68 \pm 0.01) \text{s}^{-1}$ , respectively, are 1000 fold higher in comparison to humans [43]

The GDP  $K_D$  for brown rats NDPK [45] is similar to that observed for *Sm*NDPK, while this value information for *Hs*NDPK is absent, preventing a comparison. Interestingly, the  $k_{cat}$  value is more than 300 fold smaller in comparison to all the previous results observed [46, 47].

A proteomic study has detected *Sm*NDPK in the vomitus of adult worms [40], thus suggesting a role in parasite digestion of human blood. The fact that we detected transcripts in the anterior esophagus of the parasite using WISH reinforces the idea that *Sm*NDPK might be in contact with incoming blood. A possible explanation is that extracellular ATP serves as a signal of cell distress that recruits cells involved in inflammatory responses [48]. Considering that ingested leukocytes will be under significant stress, the fact that *Sm*NDPK can convert the excess of extracellular ATP produced by such cells into other nucleotides might represent a mechanism to defuse such signaling while preserving overall level of triphosphate nucleotides for absorption and further use as energy source or metabolic components. The observed high affinity to ATP reinforces the notion that *Sm*NDPK presence in the digestive system should be related to the enzymatic breakdown of this molecule.

*Sm*NDPK is also present in a list of 463 detected in a proteomic study as exposed at the surface of recently transformed schistosomula. Considering that it is known that invading schistosomula will be met with inflammatory responses [49], proteins involved in nucleotide metabolism, such as *Sm*NDPK, could also play a role in diminishing extracellular ATP levels to avoid an exacerbated inflammatory response.

In addition, examination of previously RNA-Seq experiment measuring differential expression in adult worm gonads [39] showed *Sm*NDPK as upregulated in the ovary of paired females. In the present work, WISH using a probe for *Sm*NDPK resulted in a strongly visible signal in the gonads. We have recently identified *Sm*APRT in the ovary and vitellaria of female adult worms, where it might share with *Sm*NDPK a role in energy acquisition to support the intense egg production [50]. *Sm*NDPK, however, was also detected in the testis of male worms, suggesting a broad function related to gonads.

The *Sm*NDPK structure and kinetic activity presented here represent our latest effort to fully characterize the *S. mansoni* purine salvage pathway [50-63]. The association of *Sm*NDPK with processes related to host-parasite interaction and sexual

biology of the parasite makes it an interesting target for possible therapies, with further studies warranted to verify its potential.

## **6- Acknowledgments**

This work was funded by FAPESP, CNPq and Instituto de Física de São Carlos, Universidade de São Paulo. This work was supported by Grants 2012/14223-9 (HMP), 2012/10213-9 (JRT), 2012/23730-1 (VHBS), 2013/20715-4 (AEZ) from São Paulo Research Foundation (FAPESP) and CNPq 474402/2013-4 (HMP); 134013/2015-8 (AFF), 140636/2013-7 (VHBS) and MR/K018779/1 (LEB, JEN, RJO). Also, we would like to thank CAPES. We acknowledge Leticia Anderson and Sergio Verjovski-Almeida for providing adult *S. mansoni* worms to perform the WISH experiment.

## 7- References

- [1] R.L. Ratliff, R.H. Weaver, H.A. Lardy, S.A. Kuby, Nucleoside Triphosphate-Nucleoside Diphosphate Transphosphorylase (Nucleoside Diphosphokinase). I. Isolation of the Crystalline Enzyme from Brewers' Yeast, *J Biol Chem* 239 (1964) 301-9.
- [2] P. Berg, W.K. Joklik, Transphosphorylation between nucleoside polyphosphates, *Nature* 172(4387) (1953) 1008-9.
- [3] R.E. Parks Jr, R.P. Aganwal, 9 Nucleoside Diphosphokinases, in: D.B. Paul (Ed.), *The Enzymes*, Academic Press 1973, pp. 307-333.
- [4] J. Bourdais, R. Biondi, S. Sarfati, C. Guerreiro, I. Lascu, J. Janin, M. Veron, Cellular phosphorylation of anti-HIV nucleosides. Role of nucleoside diphosphate kinase, *J Biol Chem* 271(14) (1996) 7887-90.
- [5] S.A. Kuby, G. Fleming, T. Alber, D. Richardson, H. Takenaka, M. Hamada, Studies on yeast nucleoside triphosphate-nucleoside diphosphate transphosphorylase (nucleoside diphosphokinase). IV. Steady-state kinetic properties with thymidine nucleotides (including 3'-azido-3'-deoxythymidine analogues), *Enzyme* 45(1-2) (1991) 1-13.
- [6] C. Dumas, I. Lascu, S. Morera, P. Glaser, R. Fourme, V. Wallet, M.L. Lacombe, M. Veron, J. Janin, X-ray structure of nucleoside diphosphate kinase, *EMBO J* 11(9) (1992) 3203-8.
- [7] N. Mourad, R.E. Parks, Jr., Erythrocytic nucleoside diphosphokinase. II. Isolation and kinetics, *J Biol Chem* 241(2) (1966) 271-8.
- [8] P. Gonin, Y. Xu, L. Milon, S. Dabernat, M. Morr, R. Kumar, M.L. Lacombe, J. Janin, I. Lascu, Catalytic mechanism of nucleoside diphosphate kinase investigated using nucleotide analogues, viscosity effects, and X-ray crystallography, *Biochemistry* 38(22) (1999) 7265-72.
- [9] A. Mehta, S. Orchard, Nucleoside diphosphate kinase (NDPK, NM23, AWD): recent regulatory advances in endocytosis, metastasis, psoriasis, insulin release, fetal erythroid lineage and heart failure; translational medicine exemplified, *Mol Cell Biochem* 329(1-2) (2009) 3-15.
- [10] Y.F. Liu, A. Yang, W. Liu, C. Wang, M. Wang, L. Zhang, D. Wang, J.F. Dong, M. Li, NME2 reduces proliferation, migration and invasion of gastric cancer cells to limit metastasis, *PLoS One* 10(2) (2015) e0115968.
- [11] WORLD HEALTH ORGANIZATION, WHO - Schistosomiasis, 2017. <http://www.who.int/mediacentre/factsheets/fs115/en/>. (Accessed 02/2017 2017).
- [12] G.W. Crabtree, A.W. Senft, Pathways of nucleotide metabolism in schistosoma mansoni. V. Adenosine cleavage enzyme and effects of purine analogues on adenosine metabolism in vitro, *Biochem Pharmacol* 23(3) (1974) 649-60.
- [13] F.P. Miech, A.W. Senft, D.G. Senft, Pathways of nucleotide metabolism in Schistosoma mansoni--VI adenosine phosphorylase, *Biochem Pharmacol* 24(3) (1975) 407-11.
- [14] A.W. Senft, G.W. Crabtree, Pathways of nucleotide metabolism in Schistosoma mansoni--VII. Inhibition of adenine and guanine nucleotide synthesis by purine analogs in intact worms, *Biochem Pharmacol* 26(20) (1977) 1847-55.
- [15] A.W. Senft, G.W. Crabtree, Purine metabolism in the schistosomes: potential targets for chemotherapy, *Pharmacol Ther* 20(3) (1983) 341-56.
- [16] A.W. Senft, G.W. Crabtree, K.C. Agarwal, E.M. Scholar, R.P. Agarwal, R.E. Parks, Jr., Pathways of nucleotide metabolism in Schistosoma mansoni. 3.

- Identification of enzymes in cell-free extracts, *Biochem Pharmacol* 22(4) (1973) 449-58.
- [17] A.W. Senft, R.P. Miech, P.R. Brown, D.G. Senft, Purine metabolism in *Schistosoma mansoni*, *International journal for parasitology* 2(2) (1972) 249-60.
- [18] A.W. Senft, D.G. Senft, R.P. Miech, Pathways of nucleotide metabolism in *Schistosoma mansoni*. II. Disposition of adenosine by whole worms, *Biochem Pharmacol* 22(4) (1973) 437-47.
- [19] R.J. Stegman, A.W. Senft, P.R. Brown, R.E. Parks, Jr., Pathways of nucleotide metabolism in *Schistosoma mansoni*. IV. Incorporation of adenosine analogs in vitro, *Biochem Pharmacol* 22(4) (1973) 459-68.
- [20] H.F. Dovey, J.H. McKerrow, C.C. Wang, Purine salvage in *Schistosoma mansoni* schistosomules, *Molecular and biochemical parasitology* 11 (1984) 157-67.
- [21] W.E. Secor, D.G. Colley, *Schistosomiasis*, Springer Science + Business Media, Inc, Boston 2005.
- [22] N.S. Berrow, D. Alderton, S. Sainsbury, J. Nettleship, R. Assenberg, N. Rahman, D.I. Stuart, R.J. Owens, A versatile ligation-independent cloning method suitable for high-throughput expression screening applications, *Nucleic Acids Res* 35(6) (2007) e45.
- [23] M.J. Todd, J. Gomez, Enzyme kinetics determined using calorimetry: a general assay for enzyme activity?, *Anal Biochem* 296(2) (2001) 179-87.
- [24] N.A. Demarse, M.C. Killian, L.D. Hansen, C.F. Quinn, Determining enzyme kinetics via isothermal titration calorimetry, *Methods Mol Biol* 978 (2013) 21-30.
- [25] M.W. Freyer, E.A. Lewis, Isothermal titration calorimetry: experimental design, data analysis, and probing macromolecule/ligand binding and kinetic interactions, *Methods Cell Biol* 84 (2008) 79-113.
- [26] M.K. Transtrum, L.D. Hansen, C. Quinn, Enzyme kinetics determined by single-injection isothermal titration calorimetry, *Methods* 76 (2015) 194-200.
- [27] S.N. Olsen, E. Lumby, K. McFarland, K. Borch, P. Westh, Kinetics of enzymatic high-solid hydrolysis of lignocellulosic biomass studied by calorimetry, *Appl Biochem Biotechnol* 163(5) (2011) 626-35.
- [28] G. Winter, C.M. Lobley, S.M. Prince, Decision making in xia2, *Acta crystallographica. Section D, Biological crystallography* 69(Pt 7) (2013) 1260-73.
- [29] P.R. Evans, G.N. Murshudov, How good are my data and what is the resolution?, *Acta Crystallographica Section D-Biological Crystallography* 69 (2013) 1204-1214.
- [30] W. Kabsch, Xds, *Acta Crystallographica Section D-Biological Crystallography* 66 (2010) 125-132.
- [31] D.G. Waterman, G. Winter, R.J. Gildea, J.M. Parkhurst, A.S. Brewster, N.K. Sauter, G. Evans, Diffraction-geometry refinement in the DIALS framework, *Acta Crystallogr D Struct Biol* 72(Pt 4) (2016) 558-75.
- [32] A.J. McCoy, R.W. Grosse-Kunstleve, P.D. Adams, M.D. Winn, L.C. Storoni, R.J. Read, Phaser crystallographic software, *J Appl Crystallogr* 40(Pt 4) (2007) 658-674.
- [33] P.D. Adams, P.V. Afonine, G. Bunkoczi, V.B. Chen, I.W. Davis, N. Echols, J.J. Headd, L.W. Hung, G.J. Kapral, R.W. Grosse-Kunstleve, A.J. McCoy, N.W. Moriarty, R. Oeffner, R.J. Read, D.C. Richardson, J.S. Richardson, T.C. Terwilliger, P.H. Zwart, PHENIX: a comprehensive Python-based system for macromolecular structure solution, *Acta crystallographica. Section D, Biological crystallography* 66(Pt 2) (2010) 213-21.
- [34] P. Emsley, K. Cowtan, Coot: model-building tools for molecular graphics, *Acta Crystallogr D Biol Crystallogr* 60(Pt 12 Pt 1) (2004) 2126-32.

- [35] V.B. Chen, W.B. Arendall, 3rd, J.J. Headd, D.A. Keedy, R.M. Immormino, G.J. Kapral, L.W. Murray, J.S. Richardson, D.C. Richardson, MolProbity: all-atom structure validation for macromolecular crystallography, *Acta crystallographica. Section D, Biological crystallography* 66(Pt 1) (2010) 12-21.
- [36] A.A. Cogswell, J.J. Collins, P.A. Newmark, D.L. Williams, Whole mount in situ hybridization methodology for *Schistosoma mansoni*, *Molecular and biochemical parasitology* 178(1-2) (2011) 46-50.
- [37] G.P. Dillon, J.C. Illes, H.V. Isaacs, R.A. Wilson, Patterns of gene expression in schistosomes: localization by whole mount in situ hybridization, *Parasitology* 134(11) (2007).
- [38] F.J. Logan-Klumpler, N. De Silva, U. Boehme, M.B. Rogers, G. Velarde, J.A. McQuillan, T. Carver, M. Aslett, C. Olsen, S. Subramanian, I. Phan, C. Farris, S. Mitra, G. Ramasamy, H. Wang, A. Tivey, A. Jackson, R. Houston, J. Parkhill, M. Holden, O.S. Harb, B.P. Brunk, P.J. Myler, D. Roos, M. Carrington, D.F. Smith, C. Hertz-Fowler, M. Berriman, GeneDB--an annotation database for pathogens, *Nucleic Acids Res* 40(Database issue) (2012) D98-108.
- [39] Z. Lu, F. Sessler, N. Holroyd, S. Hahnel, T. Quack, M. Berriman, C.G. Greveling, Schistosome sex matters: a deep view into gonad-specific and pairing-dependent transcriptomes reveals a complex gender interplay, *Sci Rep* 6 (2016) 31150.
- [40] S.L. Hall, S. Braschi, M. Truscott, W. Mathieson, I.M. Cesari, R.A. Wilson, Insights into blood feeding by schistosomes from a proteomic analysis of worm vomitus, *Mol Biochem Parasit* 179(1) (2011) 18-29.
- [41] J.M. Berg, J.L. Tymoczko, L. Stryer, *Biochemistry*, 5th edition, W H Freeman, New York, 2002.
- [42] M. Brodbeck, A. Rohling, W. Wohlleben, C.J. Thompson, U. Susstrunk, Nucleoside-diphosphate kinase from *Streptomyces coelicolor*, *Eur J Biochem* 239(1) (1996) 208-13.
- [43] S.C. Lam, M.A. Packham, Isolation and kinetic studies of nucleoside diphosphokinase from human platelets and effects of cAMP phosphodiesterase inhibitors, *Biochem Pharmacol* 35(24) (1986) 4449-55.
- [44] A. Lecroisey, I. Lascu, A. Bominaar, M. Veron, M. Delepierre, Phosphorylation mechanism of nucleoside diphosphate kinase: <sup>31</sup>P-nuclear magnetic resonance studies, *Biochemistry* 34(38) (1995) 12445-50.
- [45] N. Kimura, N. Shimada, Membrane-associated nucleoside diphosphate kinase from rat liver. Purification, characterization, and comparison with cytosolic enzyme, *J Biol Chem* 263(10) (1988) 4647-53.
- [46] M. Johansson, J. Hammargren, E. Uppsäll, A. MacKenzie, C. Knorpp, The activities of nucleoside diphosphate kinase and adenylate kinase are influenced by their interaction, *Plant Science* 174(2) (2008) 192-199.
- [47] F. Georgescauld, L. Moynie, J. Habersetzer, L. Cervoni, I. Mocan, T. Borza, P. Harris, A. Dautant, I. Lascu, Intersubunit ionic interactions stabilize the nucleoside diphosphate kinase of *Mycobacterium tuberculosis*, *PLoS One* 8(3) (2013) e57867.
- [48] F. Di Virgilio, M. Vuerich, Purinergic signaling in the immune system, *Auton Neurosci* 191 (2015) 117-23.
- [49] A.P. Mountford, F. Trottein, Schistosomes in the skin: a balance between immune priming and regulation, *Trends Parasitol* 20(5) (2004) 221-6.
- [50] A.E. Zeraik, V.H. Balasco Serrao, L. Romanello, J.R. Torini, A. Cassago, R. DeMarco, H.D. Pereira, *Schistosoma mansoni* displays an adenine



phosphoribosyltransferase preferentially expressed in mature female gonads and vitelaria, *Molecular and biochemical parasitology* 214 (2017) 82-86.

[51] M.S. Castilho, M.P. Postigo, H.M. Pereira, G. Oliva, A.D. Andricopulo, Structural basis for selective inhibition of purine nucleoside phosphorylase from *Schistosoma mansoni*: kinetic and structural studies, *Bioorganic & medicinal chemistry* 18(4) (2010) 1421-7.

[52] H. D'Muniz Pereira, G. Oliva, R.C. Garratt, Purine nucleoside phosphorylase from *Schistosoma mansoni* in complex with ribose-1-phosphate, *J Synchrotron Radiat* 18(1) (2011) 62-5.

[53] A. Marques Ide, L. Romanello, R. DeMarco, H.D. Pereira, Structural and kinetic studies of *Schistosoma mansoni* adenylate kinases, *Molecular and biochemical parasitology* 185(2) (2012) 157-60.

[54] H.M. Pereira, V. Berdini, M.R. Ferri, A. Cleasby, R.C. Garratt, Crystal structure of *Schistosoma* purine nucleoside phosphorylase complexed with a novel monocyclic inhibitor, *Acta tropica* 114(2) (2010) 97-102.

[55] H.M. Pereira, A. Cleasby, S.S. Pena, G.G. Franco, R.C. Garratt, Cloning, expression and preliminary crystallographic studies of the potential drug target purine nucleoside phosphorylase from *Schistosoma mansoni*, *Acta crystallographica. Section D, Biological crystallography* 59(Pt 6) (2003) 1096-9.

[56] H.M. Pereira, M.M. Rezende, M.S. Castilho, G. Oliva, R.C. Garratt, Adenosine binding to low-molecular-weight purine nucleoside phosphorylase: the structural basis for recognition based on its complex with the enzyme from *Schistosoma mansoni*, *Acta crystallographica. Section D, Biological crystallography* 66(Pt 1) (2010) 73-9.

[57] M.P. Postigo, R. Krogh, M.F. Terni, H.M. Pereira, G. Oliva, M.S. Castilho, A.D. Andricopulo, Enzyme Kinetics, Structural Analysis and Molecular Modeling Studies on a Series of *Schistosoma mansoni* PNP Inhibitors, *Journal of the Brazilian Chemical Society* 22(3) (2011) 583-591.

[58] L. Romanello, J.F. Bachega, A. Cassago, J. Brandao-Neto, R. DeMarco, R.C. Garratt, H.D. Pereira, Adenosine kinase from *Schistosoma mansoni*: structural basis for the differential incorporation of nucleoside analogues, *Acta crystallographica. Section D, Biological crystallography* 69(Pt 1) (2013) 126-36.

[59] L. Romanello, V.H.B. Serrao, J.R. Torini, L.E. Bird, J.E. Nettleship, H. Rada, Y. Reddivari, R.J. Owens, R. DeMarco, J. Brandao-Neto, H.D. Pereira, Structural and kinetic analysis of *Schistosoma mansoni* Adenylosuccinate Lyase (SmADSL), *Molecular and biochemical parasitology* 214 (2017) 27-35.

[60] J.R. Torini, J. Brandao-Neto, R. DeMarco, H.D. Pereira, Crystal Structure of *Schistosoma mansoni* Adenosine Phosphorylase/5'-Methylthioadenosine Phosphorylase and Its Importance on Adenosine Salvage Pathway, *PLoS neglected tropical diseases* 10(12) (2016) e0005178.

[61] V.H.B. Serrao, H.D. Pereira, J.R.T. de Souza, L. Romanello, *Schistosoma mansoni* purine and pyrimidine biosynthesis: structures and kinetic experiments in the search for the best therapeutic target, *Current pharmaceutical design* (2017).

[62] H.D. Pereira, G.R. Franco, A. Cleasby, R.C. Garratt, Structures for the potential drug target purine nucleoside phosphorylase from *Schistosoma mansoni* causal agent of schistosomiasis, *Journal of molecular biology* 353(3) (2005) 584-99.

[63] J.R. Torini, L. Romanello, F.A.H. Batista, V.H.B. Serrao, M. Faheem, A.E. Zeraik, L. Bird, J. Nettleship, Y. Reddivari, R. Owens, R. DeMarco, J.C. Borges, J. Brandao-Neto, H.D. Pereira, The molecular structure of *Schistosoma mansoni* PNP isoform 2 provides insights into the nucleoside selectivity of PNPs, *PloS one* 13(9) (2018) e0203532.



**Legends:**

Table 1. Kinetics parameters from *Sm*NDPK during the binding and enzymatic assays.

Table2. Data collection, processing and refinement statistics of *Sm*NDPK.

Figure 1. Sequence alignment showing the secondary structure elements comparing *Sm*NDPK with both human homologues (*Hs*NDPK-A and *Hs*NDPK-B) generated by the Esprint server.

Figure 2. Localization of NDPK transcripts by whole mount *in situ* hybridization in adult *S. mansoni* worms. (A) Female adult worm showing strong labeling in the entire ovary (A - upper arrow) and also staining in the vitellaria (lower arrow). (B) Part of the female worm body exposed to hybridization solution containing antisense *Sm*NDPK riboprobe; strong staining in the vitellaria (arrowed) is noticeable. (C) Male adult worms presenting labeling in the testis (arrow) and anterior esophagus region (arrowhead). (D) Control female and male worms incubated with sense RNA strand.

Figure 3. The binding assays comparing of *Sm*NDPK. Multiple injection by ITC showing the binding profile for ATP, GTP, CTP, TTP, UTP and ATP $\gamma$ S (A to F), respectively, also as negative control: Bovine Serum Albumin (BSA) interacting with ATP and ATP $\gamma$ S (G and H) was used as negative control. The kinetics parameters are showed in Table 1.

Figure 4. The binding assays in presence of non-hydrolysable ATP $\gamma$ S. Multiple injection by ITC showing the binding profile for ADP, GDP, CDP, TDP and UDP (A to E), respectively. The kinetics parameters are showed in Table 1.

Figure 5. *Sm*NDPK structure. (A) The macromolecular assembly observed in the asymmetric unit revealed the canonical hexamer oligomerization, or a dimer of trimers. (B) The monomer topology shows a canonical Nucleoside diphosphate kinase-like domain (CATH 3.30.70.141), or an alpha-beta 2-layers sandwich.

Figure 6. Analysis of the *Sm*NDPK.ADP complex. (A) Composit omit map countered at 1.7 sigma of ADP molecules in the *Sm*NDPK active site. (B) Active site of *Sm*NDPK with bound ADP. (C) The ligand-plot schematic generated by the Lidia software. Highlighting the important residues responsible for the “ping-pong” catalysis [3], as the H115, not involved directly into the binding, but being crucial for the kinetic effect in this enzyme class.

**Table 1.**

| <u>Binding assays</u>              |                        |                                   | HMDB                     | <u>Kinetics assays</u>                |                        |
|------------------------------------|------------------------|-----------------------------------|--------------------------|---------------------------------------|------------------------|
|                                    | $K_D^{avg}$ ( $\mu$ M) | $\Delta H_{app}^{avg}$ (kcal/mol) | concentration ( $\mu$ M) | $K_M$ ( $\mu$ M)                      | $k_{cat}$ ( $s^{-1}$ ) |
| <b>ATP</b>                         | $3.10 \pm 0.02$        | $+(3.3 \pm 0.3)$                  | $> 1300$                 | -                                     | -                      |
| <b>GTP</b>                         | $3.30 \pm 0.07$        | $-(3.0 \pm 0.7)$                  | $56.0 \pm 7.0$           | -                                     | -                      |
| <b>CTP</b>                         | -                      | -                                 | 28.0                     | -                                     | -                      |
| <b>TTP</b>                         | $10.0 \pm 1.6$         | $-(2.3 \pm 0.1)$                  | -                        | -                                     | -                      |
| <b>UTP</b>                         | $9.9 \pm 1.3$          | $-(9.8 \pm 5.1)$                  | -                        | -                                     | -                      |
| <b>ATP<math>\gamma</math>S</b>     | $7.25 \pm 0.42$        | $-(3.9 \pm 0.8)$                  | -                        | -                                     | -                      |
| <b>ADP</b>                         | $1.45 \pm 0.06$        | $-(1.7 \pm 0.1)$                  | $160.0 \pm 14.0$         | $\Delta H_{ATP/GDP} = + 2.0$ kcal/mol |                        |
| <b>GDP</b>                         | $9.99 \pm 0.05$        | $-(1.4 \pm 0.1)$                  | $15.0 \pm 2.0$           | $36.3 \pm 1.6$                        | $0.68 \pm 0.01$        |
| <b>ATP<math>\gamma</math>S CDP</b> | $10 \pm 5$             | $-(9.6 \pm 2)$                    | $36.0 \pm 12.0$          | -                                     | -                      |
| <b>TDP</b>                         | $9.9 \pm 0.4$          | $-(14.4 \pm 0.4)$                 | -                        | -                                     | -                      |
| <b>UDP</b>                         | $9.4 \pm 0.4$          | $-(17.3 \pm 2.7)$                 | $41.0 \pm 12.0$          | -                                     | -                      |

**Table 2.**

|                                 | <i>SmNDPK-apo-C<sub>2</sub></i> | <i>SmNDPK-apo P6<sub>3</sub>22</i> | <i>SmNDPK-ADP</i>  |
|---------------------------------|---------------------------------|------------------------------------|--------------------|
| Detector                        | Pilatus 2M                      | Pilatus 2M                         | Pilatus 2M         |
| Cell parameters (Å)             | 211.76;                         |                                    | 71.45; 71.45;      |
| a; b;c                          | 82.27; 122.37                   | 71.59; 71.59; 219.44               | 219.34             |
|                                 | 90; 104.89; 90                  | 90; 90; 120                        | 90; 90; 120        |
| Space Group                     | C2                              | P6 <sub>3</sub> 22                 | P6 <sub>3</sub> 22 |
| Resolution (Å)                  | 59.1- 1.74                      | 47.30 - 1.90 (1.95-                | 61.8- 2.11         |
|                                 | (1.79-1.74)                     | 1.90)                              | (2.16 -2.11)       |
| X-ray Source                    | I04-1                           | I04-1                              | I04-1              |
| $\lambda$ (Å)                   | 0.92                            | 0.92                               | 0.92               |
| Multiplicity                    | 3.4 (3.3)                       | 9.6 (10.0)                         | 18.9 (19.6)        |
| R <sub>merge</sub> (%)          | 7.0 (70.4)                      | 10.4 (70.4)                        | 8.5 (71.0)         |
| R <sub>pim</sub> (%)            | 4.4 (45.9)                      | 3.5 (23.1)                         | 2.0 (16.4)         |
| CC(1/2)                         | 0.997 (0.6440)                  | 0.998 (0.846)                      | 1.0 (0.936)        |
| Completeness (%)                | 98.4 (98.3)                     | 99.6 (98.6 - 99.5)                 | 100 (99.4 - 100 )  |
| Reflections                     | 695442                          | 261734 (19271)                     | 379170             |
|                                 | (49438)                         |                                    | (28386)            |
| Unique Reflections              | 204192                          | 27155 (1934)                       | 20075 (1450)       |
|                                 | (15018)                         |                                    |                    |
| I/ $\sigma$                     | 11.2 (1.9)                      | 15.3 (3.6)                         | 27.7 (5.1)         |
| Reflections used for Refinement | 204169                          | 27125                              | 20023              |
| R(%)**                          | 16.44                           | 16.21                              | 16.82              |
| R <sub>free</sub> (%)**         | 19.09                           | 20.77                              | 19.87              |
| N° of protein atoms             | 14205                           | 2372                               | 2353               |
| N° of ligant atoms              | 0                               | 0                                  | 54                 |
| B (Å <sup>2</sup> )             | 21.60                           | 23.07                              | 36.28              |
| B (Å <sup>2</sup> ) ADP         | -                               | -                                  | 77.27              |
| Coordinate Error (ML based) (Å) | 0.20                            | 0.18                               | 0.19               |
| Phase error (°)                 | 19.29                           | 19.46                              | 19.04              |
| <i>Ramachandran Plot</i>        |                                 |                                    |                    |
| Favored (%)                     | 97.29                           | 97.64                              | 97.97              |
| Allowed (%)                     | 1.97                            | 1.68                               | 1.36               |
| Outliers (%)                    | 0.73                            | 0.67                               | 0.68               |
| All-atom Clashscore             | 2.33                            | 1.69                               | 3.15               |
| <i>RMSD from ideal geometry</i> |                                 |                                    |                    |
| r.m.s. bond lengths (Å)         | 0.005                           | 0.011                              | 0.007              |
| r.m.s. bond angles (°)          | 0.716                           | 1.023                              | 0.962              |
| <i>PDB ID</i>                   | 5IOL                            | 5IOM                               | 5KK8               |

Figure 1

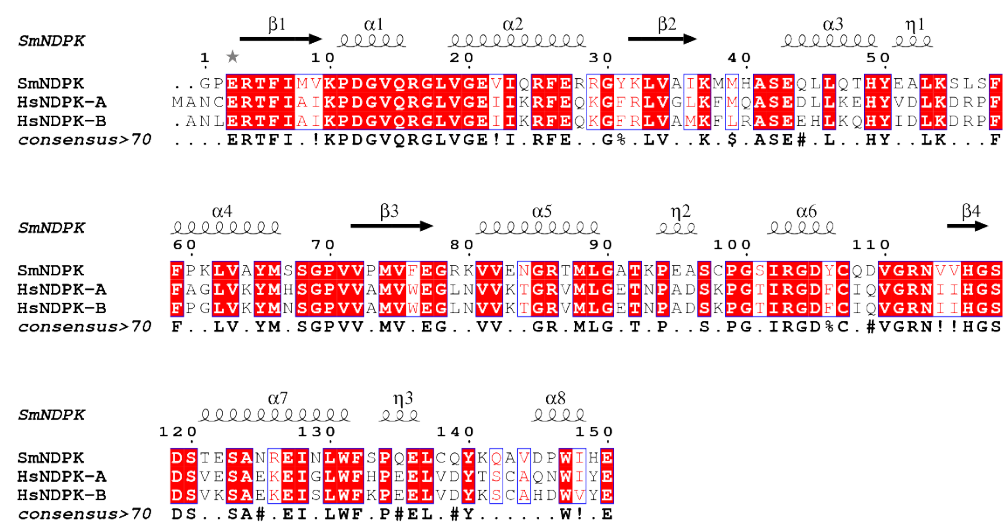
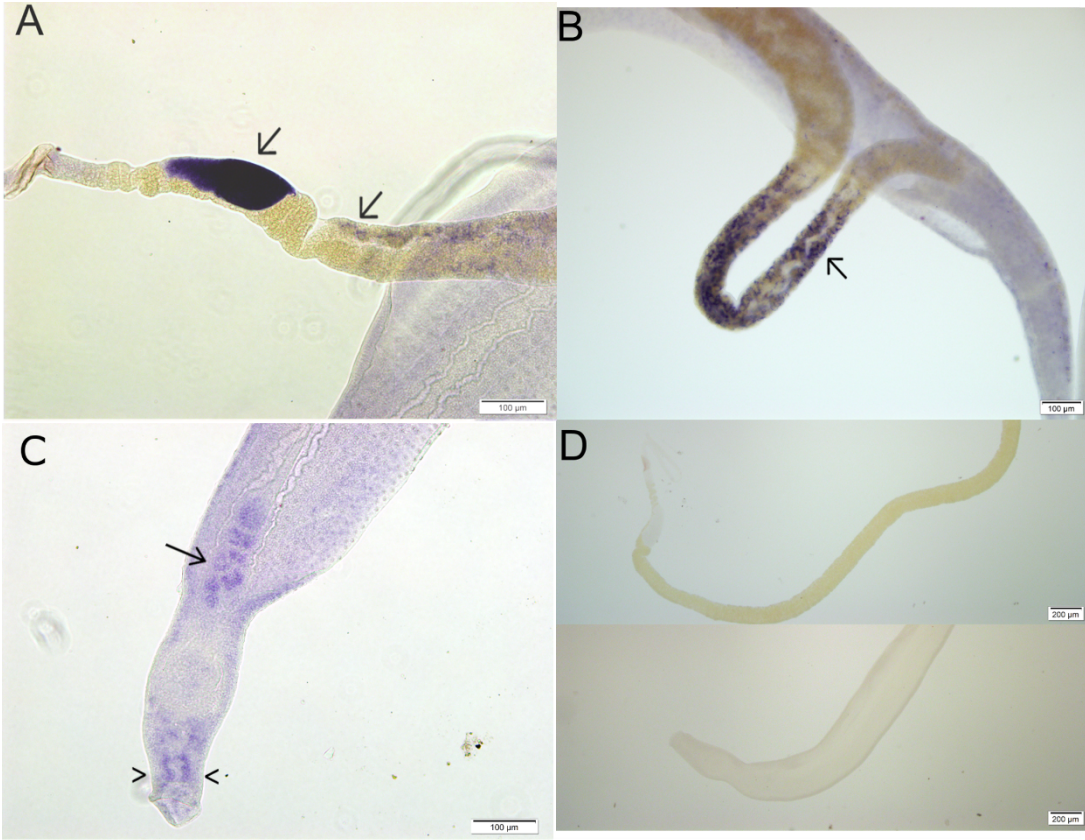
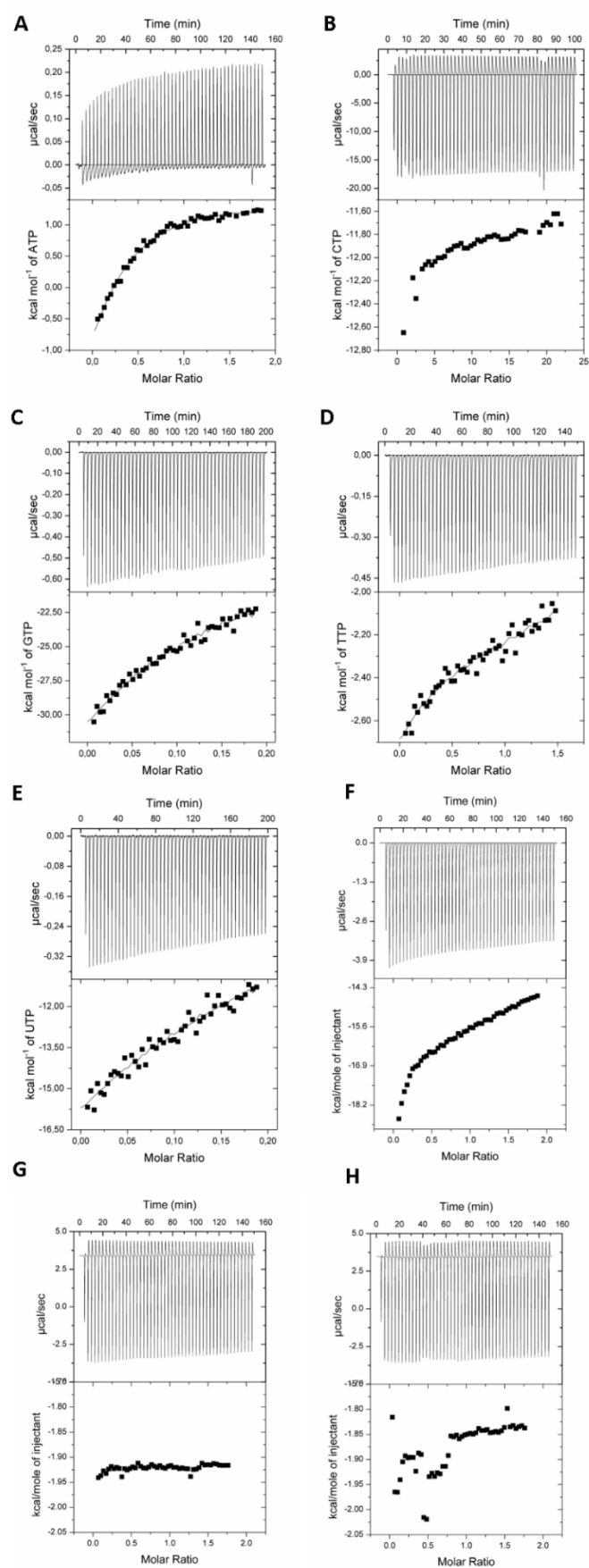


Figure 2



**Figure 3**



**Figure 4**

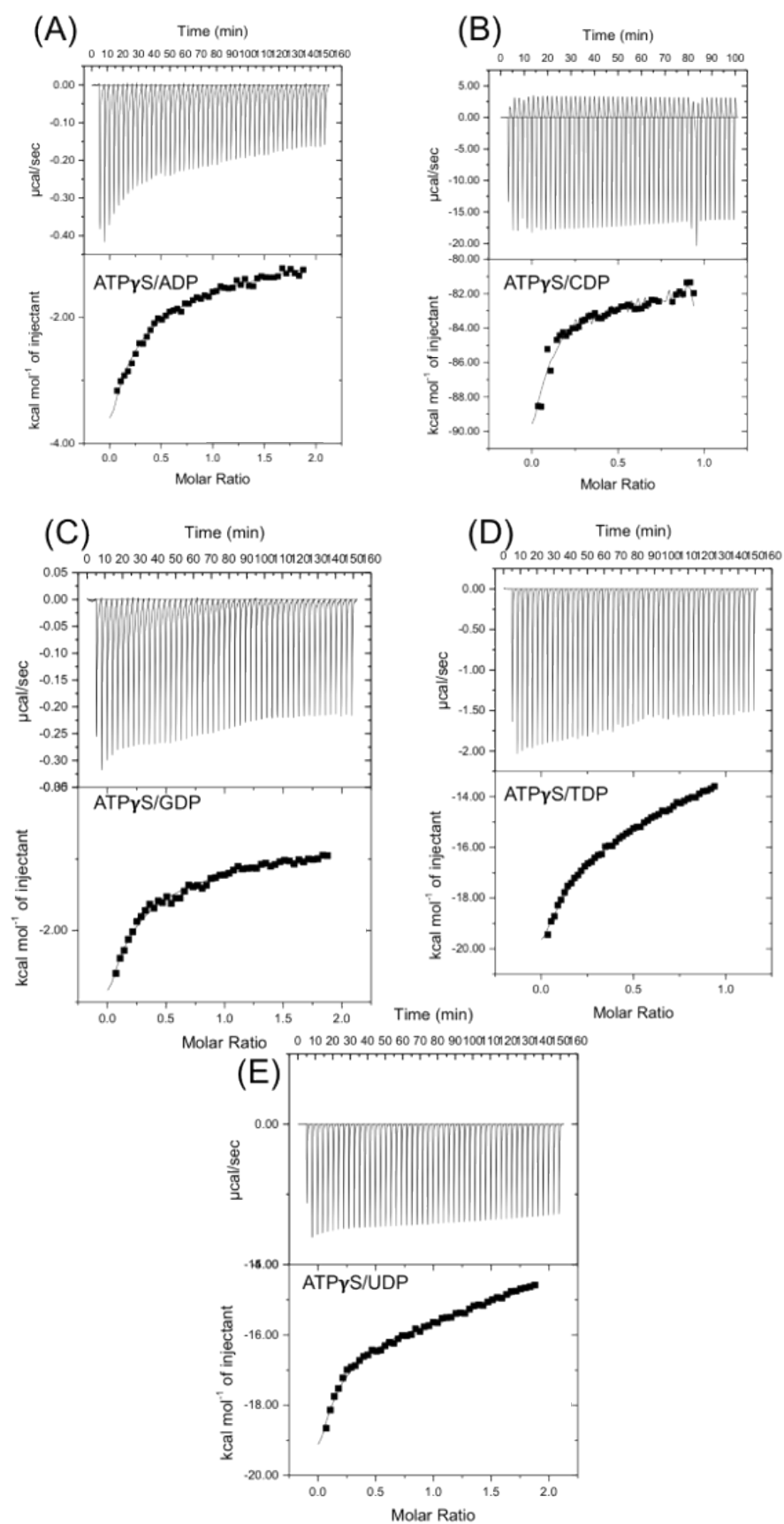




**Figure 5**

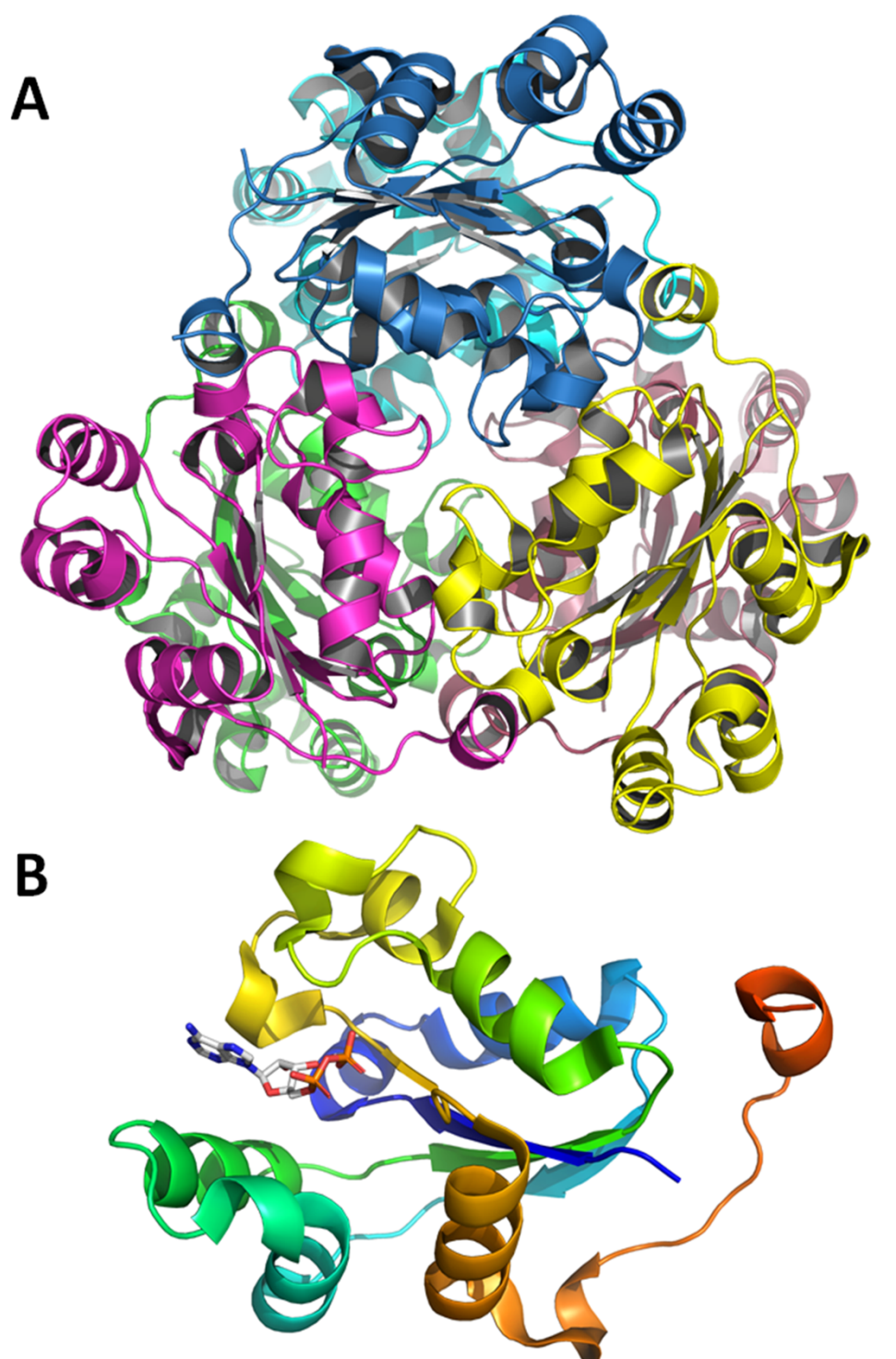
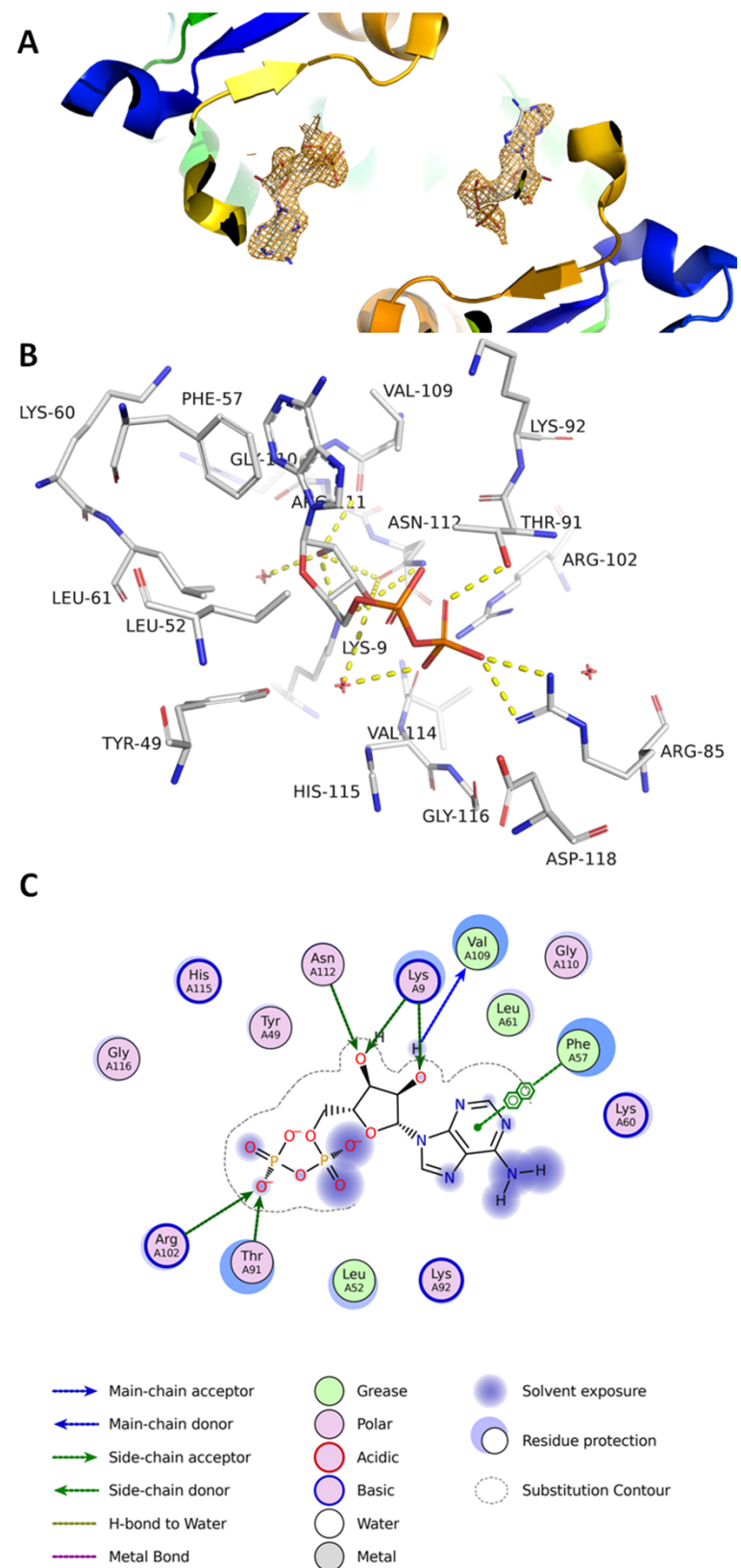


Figure 6





## Characterization of a *Schistosoma mansoni* NDPK expressed in sexual and digestive organs

Juliana Roberta Torini<sup>1†</sup>, Adriano de Freitas Fernandes<sup>1†</sup>, Vitor Hugo Balasco Serrão<sup>1,2†\*</sup>, Larissa Romanello<sup>1</sup>, Louise E Bird<sup>3</sup>, Joanne E Nettleship<sup>3</sup>, Raymond J Owens<sup>3</sup>, José Brandão-Neto<sup>4</sup>, Ana Eliza Zeraik<sup>1</sup>, Ricardo DeMarco<sup>1</sup>, Humberto D'Muniz Pereira<sup>1</sup>.

1- Laboratório de Biologia Estrutural, Instituto de Física de São Carlos, Universidade de São Paulo, 13563-120, São Carlos, SP, Brazil. 2-Department of Medicine Pathobiology, University of Toronto, M5S 1A8, Toronto, Canada. 4- OPPE-UK, Research Complex at Harwell, Rutherford Appleton Laboratory, Oxford, OX11 0FA, UK. 5-Diamond Light Source, Harwell Science and Innovation Campus, Didcot, Oxfordshire, OX11 0DE, UK.

<sup>†</sup> The authors contribute equality to this work.

\*To whom correspondence should be addressed: Dr. Vitor Hugo Balasco Serrão, Department of Medicine Pathobiology, University of Toronto, 1 King's College Circle, M5S 1A8. Toronto, ON, Canada, Telephone (+1) 647-996-3914; e-mail: vitor.serrao@utoronto.ca

Keywords: Crystallography; Isothermal Titration Calorimetry; NDPK, *Schistosoma mansoni*

This work was supported by Grants 2012/14223-9 (HMP), 2012/10213-9 (JRT) 2012/23730-1 (VHBS) from São Paulo Research Foundation (FAPESP) and CNPq 474402/2013-4 (HMP); 134013/2015-8 (AFF), 140636/2013-7 (VHBS) and MR/K018779/1 (LEB, JEN, RJO). Also, we would like to thank CAPES.

## Abstract

Nucleoside diphosphate kinases (NDPKs) are crucial to keep the high triphosphate nucleotide levels in the biological process. The enzymatic mechanism has been extensively described; however, the structural characteristics and kinetic parameters have never been fully determined. In *Schistosoma mansoni*, NDPK (*Sm*NDPK) is directly involved in the pyrimidine and purine salvage pathways, being essential for nucleotide metabolism. The *Sm*NDPK enzymatic activity is the highest of the known purine metabolisms when compared to the mammalian NDPKs, suggesting the importance of this enzyme in the worm metabolism. Here, we report the recombinant expression of *Sm*NDPK that resulted in 1.7 and 1.9 Å apo-form structure in different space-groups, as well as the 2.1 Å *Sm*NDPK.ADP complex. The binding and kinetic assays reveal the ATP-dependence for enzyme activation. Moreover, *in situ* hybridization showed that *Sm*NDPK transcripts are found in reproductive organs and in the esophagus gland of adult worms, which can be intrinsically related with the oviposition and digestive processes. These results will help us fully understand the crucial participation of this enzyme in *Schistosoma mansoni* and its importance for the pathology of the disease.

## 2- Introduction

Nucleoside diphosphate kinase (EC2.7.4.6) is the enzyme responsible for the reversible transference of  $\gamma$ -phosphoryl group from a triphosphate to a diphosphate nucleoside [1, 2]. This transfer mechanism occurs through a enzymatic transitory state, where a catalytic histidine is temporarily phosphorylated, creating a “*ping-pong*” mechanism [3], as can be seen at schema below:



The NDPK is found in all cells and it is able to use both purines and pyrimidines nucleotides, as well as oxy and deoxy derivates, showing low specificity to bases moiety of the nucleotides [4, 5]. These characteristics confer an important role on the balance and maintenance of oxy- and deoxy triphosphate nucleoside into cells [6-8] and could be related with cardiovascular disease [9] and problems during the metastasis processes [10].

Due to their importance in cell metabolism, many structural studies have been performed (154 PDB entries). Interestingly, in only a few the native substrates (ADP, ATP, CDP, CTP, GDP, dGTP/GTP, TDP, and UDP) were used.

The *S. mansoni* parasite is an atypical trematode (the adult stage is sexually dimorphics); it is the causative agent of schistosomiasis, a neglected tropical disease that, according to Word Health Organization, affects 218 million of people worldwide [11]. *S. mansoni* is incapable of synthesizing purine nucleotides or their immediate precursors by the *de novo* pathway [12-20], thus the purine salvage pathway represents a vital pathway for the maintenance of ATP or GTP energy systems, with NDPK occupying a central position in the control of cell functions.

This enzyme is important in several biological processes from bacteria to humans. In the *Schistosoma mansoni* parasite, NDPK activity is the highest of the purine metabolism in adult schistosomes crude extracts, and when compared with mammalian tissues, is 5 to 10 fold greater in *S. mansoni* [16], indicating that NDPK activity is even more pronounced in the parasite metabolism.

Here, we describe the three-dimensional structure of NDPK from *Schistosoma mansoni* (SmNDPK) obtained by protein crystallography. In addition, nucleotide binding assays using a non-hydrolysable phosphate donor were conducted by

Isothermal Titration Calorimetry, showing the sequential binding preference. Finally, we show the localization of *SmNDPK* transcripts in the gonads and anterior esophagus of adult worms by whole-mount *in situ* hybridization (WISH). Therefore, it is possible to hypothesize that *SmNDPK* is particularly important to parasite reproduction and digestion. The predominant localization in the ovaries of female adult worms makes this protein likely to be involved in the oviposition process, which is a key pathology feature in the development and transmission of the disease [21].

### 3- Materials and Methods

#### *Cloning, Expression, and purification of recombinant SmNDPK*

The *SmNDPK*(*Smp\_092750*) gene was synthesized with codon optimization by GenScript company and cloned into pOPINF[22] using the *In-Fusion* method (Clontech, Mountain View, CA, United States). pOPINF-*Smndpk* vector was transformed into Omni-MaxII cells (Invitrogen), transformants were selected using the chromogenic substrate X-Gal and by colony PCR, white colonies were picked and grown in Power Broth™ medium supplemented with 50 µg/mL of carbenicillin antibiotic at 37 °C and 600 rpm for 16 hours. The plasmid mini-preps were performed on the *Onyx* robotic system according to the manufacturer's protocols. The purified plasmid (pOPINF-*Smndpk*) was used in the transformation of *Escherichia coli* Rosetta2™ (DE3) strain. The protein was expressed using Power Broth™ medium supplemented with 50 µg/mL of carbenicillin and 35 µg/mL chloramphenicol. The cells were incubated at 37 °C for 4 hours to OD<sub>600</sub> of about 0.5 and induced with 0.1 mM of isopropyl β-D-1-thiogalactopyranoside (IPTG), then were incubated at 18 °C for 16 hours with continuous shaking at 250 rpm, harvested by centrifugation at 5000g for 15 minutes and frozen at -20 °C.

The cells were defrosted and lysed in a different lysis buffer (50 mM potassium phosphate pH 7.6, 300 mM NaCl, 10 mM imidazole, 5 mM 2-mercaptoethanol, 0.1 mM dithiothreitol (DTT) and 1 mM phenylmethylsulphonyl fluoride (PMSF). The cells were lysed by sonication followed by centrifugation (4700 g for 40 min. at 4 °C). The clarified lysate was applied to Co<sup>2+</sup>-agarose column (Qiagen), after column wash, the 6His-*SmNDPK* was step-eluted with elution buffer (50 mM potassium phosphate pH 7.6, 300 mM NaCl, 200 mM imidazole and 5 mM 2-mercaptoethanol).

The 6-His-Tag was cleaved by addition of 3C protease (1 U/100 µg fusion protein) with overnight incubation at 4 °C. Cleaved *SmNDPK* was purified from the digest using a reverse purification in Ni<sup>2+</sup>-NTA column. The eluate was then concentrated and followed by dialysis in appropriate buffer to further studies. All steps from expression were analyzed by SDS-PAGE 15%.

### ***Binding and Kinetic Assays by Isothermal Titration Calorimetry***

The *Sm*NDPK binding assays during the nucleotides recognition were performed by isothermal titration calorimetry (ITC) experiments with titration in a VP-ITC calorimeter [23]. The apparent molar enthalpy ( $\Delta H_{app}$ ) from each interaction was monitored by sequential titrations from the triphosphate nucleotides (ATP, CTP, GTP, TTP, UTP and non-hydrolysable nucleotide - ATP $\gamma$ S) as recognized as substrates for NDPKs.

*Sm*NDPK was prepared in phosphate buffer (50 mM potassium phosphate pH 7.6, 150 mM NaCl, 1 mM MgCl<sub>2</sub>) and 100  $\mu$ M were placed in the VP-ITC experimental cell. The nucleotides (Sigma-Aldrich) were prepared at 1 mM by dilution in the same buffer and titrated using multiple injections (2  $\mu$ L each) at 25 °C and monitored the heat exchange during 160 s. These substrates were titrated by 20-35 injections with a stirring speed of 300 rpm [24, 25]. The  $\Delta H_{app}$  was obtained by integration of the area under the peak yields after subtracting the heat of dilution from the nucleotides [24, 26].


For monitoring the diphosphate nucleotides binding, the same procedure was performed using the same experimental procedures. However, the results showed inexpressive binding results (no detectable heat exchange), revealing no binding to diphosphate nucleotides. Then, the diphosphate nucleotides binding assays were performed using 1 mM ATP $\gamma$ S as excess placed at cell and syringe during the titrations. The initial *Sm*NDPK.ATP $\gamma$ S complex was evaluated in order to understand the preference and capability to recognize and bind to the diphosphate nucleotides. The results were processed using the Origin 7.0 software associated to the microcalorimeter, and the integral of the curve obtained reflects the heat variation in the system using sequential binding site model ( $n = 6$ ) to perform the best fit considering that *Sm*NDPK is a hexamer in solution. All the results were determined by triplicate measurements. Binding using bovine serum albumin (BSA, Sigma-Aldrich A2153) was used as negative control being performed at the same experimental conditions.

In addition, the *Sm*NDPK enzymatic assay to determine the kinetics parameters of GDP phosphorylation by ATP consumption was also performed by ITC. In spite of NDPKs enzymes present a “*ping-pong*” reaction mechanism, the fast

reaction treatment from the single-injection assays may help to infer the kinetics parameters [26].

To measure the apparent molar enthalpy ( $\Delta H_{app}$ ), 2  $\mu$ M *Sm*NDPK was titrated with a fast injection (2.5 seconds) with 20  $\mu$ L ATP (1 mM), at 15 °C and the heat exchange was monitored for 1200 seconds. Enzyme and ATP were prepared in phosphate buffer (50 mM potassium phosphate pH 7.6, 150 mM NaCl, 1 mM  $MgCl_2$ ) containing 1 mM of GDP. After ATP heat dilution subtraction, it was possible to obtain the  $\Delta H_{app}$  by the integration of the area under the peak yields [24, 26].

The results were also processed using Origin 7.0 where the integral of the curve obtained reflects the heat variation in the system and the kinetic parameters were determined by the Michaelis-Menten model applied to single-peak analysis [27].

  
A crystallization screen (OPPF-UK) was performed (using *Sm*NDPK prepared in Tris buffer), to determinate the optimal concentration of sample for setting up the crystallization experiments. Using *Sm*NDPK at 5mg/mL, crystallization screening experiments were performed in OPF-UK on Cartesian 2 using screen solutions from Molecular Dimension (Morpheus® and JCSG-*plus*™), Hampton Research (Index HT™) and Jena Bioscience (JBScreen Wizard 1 and JBScreen Wizard 2) using sitting drop.

For co-crystallization experiments, the *Sm*NDPK was incubated with 5mM of each ligand (ADP, ATP, and GDP), and submitted to crystallization trials with 1:1  $\mu$ L drops in a Honeybee 961 robot in Greiner Crystal Quick plates and incubated at 18 °C. Different crystals forms appear after two days and reach their maximum size (~150 $\mu$ m).

The crystals were mounted in microloops, cooled with 20% glycerol or PEG200 and frozen in liquid nitrogen. Diffraction data were measured using synchrotron radiation at beamline I04-1 of the Diamond Light Source (DLS, Harwell, UK). The data were indexed, integrated and scaled using the Xia2 [28-31].

The *Sm*NDPK-apo enzyme structure was solved by molecular replacement using the Phaser program [32], employing NDPK enzyme from *Drosophila melanogaster* (PDB.ID:1NDL) which shares 62% identity as a search model. The remaining structures were also solved by molecular replacement, using as model one

of the structures previously refined. The refinement was carried out using Phenix[33] and the model building performed COOT [34], using a weighted 2Fo–Fc and Fo–Fc electron density maps. In all cases the behavior of R and  $R_{\text{free}}$  was used as the principal criterion for validating the refinement protocol and the stereochemical quality of the model was evaluated with Molprobity [35]. The coordinates and structure factors have been deposited with the PDB under the following codes: *Sm*NDPK-apo ( $C_2$ symmetry) – 5IOL, *Sm*NDPK-apo ( $P6_322$ symmetry) –5IOM, and *Sm*NDPK.ADP complex – 5KK8.

### ***Whole-mount in situ hybridization (WISH)***

A fragment spanning 300 bp of *S. mansoni* NDPK was amplified from adult worm's cDNA, using the following primers: *Sm*NDPK\_Foward primer: 5'-ATGGAACGGACGTTTATTATGG-3' and *Sm*NDPK\_Reverse primer: 5'-TGATCCAGGACAACCTTGCTTC-3'. The amplicon was inserted into a pGEM-T Easy vector (Promega) and sequenced to confirm the amplicon identity as well as the orientation of the strands into the vector. Riboprobe kit (Promega) was used to produce sense or anti-sense Digoxigenin(DIG)-labelled RNA probes, following manufacturer's instructions. Whole-mount *in situ* hybridization (WISH) experiment was carried out as previously described [36, 37]. In brief, *S. mansoni* adult worms were fixed in Carnoy's fixative (ethanol:chloroform: glacial acetic acid in a 6:3:1 ratio) on ice for 2 h, followed by fixation in MEMFA (0.1 M MOPS pH 7.4, 2 mM EGTA, 1 mM  $MgSO_4$ , 3.7% formaldehyde) for 1 h and then washed and stored in 100% ethanol at -20 °C. The worms were permeabilized with proteinase K (Roche) after being rehydrated through a methanol series to PBS with 0.3% Triton-X 100 (PBSTx) and then were post-fixed in 4% paraformaldehyde (PFA). Hybridization was performed with 1  $\mu$ g/mL of antisense DIG-labelled RNA probe in hybridization buffer (50% formamide, 5 X SSC, 1% Tween-20 and 1 mg/mL of RNA from torula yeast) at 56 °C for 18-20 h. The control group was incubated with the DIG-RNA probe corresponding to the sense strand of *Sm*NDPK. The worms were then extensively washed and incubated in blocking solution (100 mM maleic acid, 150 mM NaCl, 0.1% Tween-20, pH 7.5 containing 10% horse serum) for 2 h at room temperature before the incubation with anti-DIG-alkaline phosphatase-conjugated antibody (Roche) diluted in blocking solution (1:2000), carried out at 4 °C for 16 h.



The signal was developed by nitro-blue tetrazolium chloride (NBT) and 5-Bromo-4-chloro-3'-indolylphosphate p-toluidine (BCIP) solutions (Roche). Specimens were imaged an Olympus BX53 microscope.

## 4- RESULTS AND DISCUSSIONS

### *SmNDPK sequence analysis and expression in adult worms*

A search on *S. mansoni* genome available on GeneDB[38] allowed the detection of five annotated NDPK genes. We selected one gene (*Smp\_092750*, which we named *SmNDPK*) coding for the *S. mansoni* NDPK displaying the highest identity with the previously described NDPKs from humans for further studies (~60% identity to both *HsNDPK-A* and *HsNDPK-B*, Fig. 1).

The expression levels of this gene, calculated from RNA-Seq libraries of different life cycle stages and available on GeneDB, reveal that the *SmNDPK* expression in adult worms are approximately 3-fold higher than that of cercariae and 24 h-cultured schistosomula and 9-fold higher than 3 h cultured schistosomula. The localization of *SmNDPK* transcripts in adult worms was determined by WISH experiments and showed strong labeling in the ovary and vitellaria of female adult worms (arrows in Fig 2A and B). Male adult worms displayed staining in the testes (arrow in Fig 2C). No staining was observed in the control group, incubated with *SmNDPK* sense riboprobe (Fig 2D). This reinforces the idea that the main function of this protein is associated with the mature sexual apparatus of adult worms, since inspection of data from a previously described RNA-Seq analysis from gonads of *S. mansoni* adult worms [39] reveals that *SmNDPK* is upregulated in ovaries of paired females in comparison with unpaired females. Apart from the strong labeling observed in the reproductive organs of adult worms, labeling in the anterior region of the esophagus was also detected (Fig 2C arrow head). This appears to confirm a previous proteomic analysis of worm vomitus [40] that suggested that *SmNDPK* was involved in parasite digestion of host blood.

The *SmNDPK* codes a protein with 149 amino acids with a molecular weight of about 17 kDa that was successfully expressed in a heterologous system using pOPINF vector and purified, yielding 12 mg per liter of culture medium. Retention times in an analytical size exclusion chromatography of the purified protein suggested a hexameric conformation in solution (~120 kDa, data not shown), which is a common feature of NDPKs.

### ***Binding and Kinetics Assays***

Parks and Agarwal described NDPK enzyme [3] displaying many different substrates, where the general reaction is via “*ping-pong*” mechanism, as follows:  $\text{XDP} + \text{YTP} \leftrightarrow \text{XTP} + \text{YDP}$  (X and Y each represent different nitrogenous base). NDPKs activities maintain an equilibrium between the concentrations of different nucleoside triphosphates [41].

The binding assays using Isothermal Titration Calorimetry (ITC) with several nucleotides (Fig 3A-E) showed higher affinity for ATP and GTP with dissociation constants of 3.1 and 3.3  $\mu\text{M}$ , respectively. The other nucleotides tested showed significantly higher dissociation constants (Table 1). The ATP $\gamma$ S nucleotide also presented a binding profile with dissociation constant of  $(7.25 \pm 0.42) \mu\text{M}$ . BSA was used as negative control (Fig. 3G-H).

These results correlate with the described high availability in blood of adenine and guanine nucleotides based on Human Metabolome Database, HMDB ( $> 1300$  and  $\sim 56 \mu\text{M}$ , respectively) when compared with CTP, and both non-quantified nucleotides: TTP and UTP. Although ambiguous, the nucleotides concentrations in the bloodstream can be discrepant and vary from 28 up to 11,000 nmol/L depending on the procedures and experimental analysis.

Moreover, the promiscuities for the  $\gamma$ -phosphate donor, possibly using ATP or GTP, is evident based on the dissociation constants obtained; these results agree with the first proposal that *Sm*NDPK could use both as a phosphate donor [3].

On the other hand, the same procedure was performed for monitoring the diphosphate nucleotides binding. However, the results suggest an insignificant binding (data not shown).

The same assay using protein samples in a solution with 1 mM ATP $\gamma$ S (non-hydrolyzed nucleotide) alone and sequentially adding the diphosphate nucleotides, revealed that *Sm*NDPK displays higher affinity for these dinucleotides when previously bound to a trinucleotide (Fig 4A-E). The experiment using ADP revealed an exothermal interaction, which possibly indicated the formation of a ternary complex *Sm*NDPK:ATP $\gamma$ S:ADP, with high affinity ( $K_D = 1.45 \pm 0.06 \mu\text{M}$ ), about 8 times smaller than the same experiment using other dinucleotides (Table 1). The enzymatic activity of *Sm*NDPK was characterized as an endothermic reaction with enthalpy exchange reaction of  $\Delta H_{\text{ATP/GDP}} = + 2.0 \text{ kcal/mol}$  by a single injection ITC

under saturating conditions (data not shown). Further characterization by fast reaction analysis based on the single injection peak shows the  $K_M = (36.3 \pm 1.6) \mu\text{M}$  and  $k_{\text{cat}} = (0.68 \pm 0.01) \text{ s}^{-1}$  to ATP consumption and GTP formation (Table 1) obtained by Michaelis-Menten fit.

ATP affinity is similar to the previously described affinity for *Streptomyces coelicolor* [42] and 1000 fold higher than the affinity observed for human NDPK [43]. This high affinity might be connected with necessity for ATP absorption directly from the blood, being driven to keep the worm nucleotide metabolism from the absorbed ATP.

However, the GTP affinity is 20-fold higher than any of the previous NDPKs described on BRENDA database.

### ***SmNDPK structure***

Three *SmNDPK* structures were obtained: Apo structures in  $C_2$ ;  $P_6322$  space groups and *SmNDPK* ADP complex in  $P_6322$  space group. The  $P_6322$  structure has two molecules per asymmetric unit and the  $C_2$  structure in space group has twelve molecules per asymmetric unit, forming two full hexamers. The X-ray data were collected in beamline I04-1 of the Diamond Light Source (UK) and used to obtain three-dimensional structures with resolution ranging from 1.79 Å (*SmNDPK*-apo  $C_2$ ) to 2.1 Å (*SmNDPK*-ADP). The data collection and refinement statistics can be seen in Table 2.

The *SmNDPK*'s functional unit is a hexamer as observed in other eukaryotic species (Fig 5A) and can be viewed as the stacking of two trimers. The *SmNDPK* monomer is composed by an  $\alpha/\beta$  domains, a central beta sheet with four antiparallel beta-strand ( $\beta_2$ ,  $\beta_3$ ,  $\beta_1$  e  $\beta_4$ ) surrounded by eleven alpha helices (Fig 5B).

All  $\alpha$ -helices, and  $\beta$  sheets positions are conserved with exception of a helix arrangement between residues 108 to 112 in humans.

A comparison of the structure with different ligands resulted in a maximum RMSD between chain A from *SmNDPK*-apo  $P_6322$  and chain L from *SmNDPK*-apo  $C_2$  structures (Root mean-square deviation, RMSD 0.227 Å). This indicates that the ligand does not induce significant structural changes. The overlap of monomers from the structures obtained showed that the side chain positions of residues are broadly conserved; conformational changes are noted mainly in the side chains of the F57,

E121, L129, Q134, Q138 and K140 residues. The monomer B from *Sm*NDPK-apo C2 shows the highest number of residues with conformational changes in their side chains, along with a slight loop deviation (between L53 and F58 residues) of 2.6 Å.

The RMSD of *Sm*NDPK relative to human NDPK-A (PDB.ID 2HVD) and NDPK-B (PDB.ID 1NUE) is 0.573 Å and 0.398 Å, respectively. The main difference between the structure from schistosome and human proteins happens between Q111-N115 residues (corresponding to D108-N112 in *S. mansoni* NDPK), where there is a small  $\alpha$ -helix that is not present in *Sm*NDPK.

### Active site analysis

Analysis of the crystal structure from *Sm*NDPK allowed the characterization of the active site due to the ADP presence; the residues involved in its binding are conserved. In Fig 6, residues that belong to the catalytic pocket and nucleotide binding are shown (Fig. 6A-C). However, the main residues, responsible for the catalytic activity of the enzyme are away from the binding cleft. These residues determine the sequence HGS (H115, G116, and S117), that is conserved in all existing NDPKs (Fig 6C).

These HGS residues form the catalytic pocket exposed to solvent; there are no residues from neighboring subunits involved in the nucleotide binding. The direct interaction with ADP molecule occurs between the ribose portion and K9, T91, V109 and N112 residues. However, four other residues (L52; F57; L61; R102) collaborate, thus, stabilizing the purine portion. The NDPKs have low specificity to the base portion of nucleotides; the base binding happens inside of a hydrophobic cleft of the active site and, therefore, displays weak interactions with the protein.

This weak interaction with the base justifies the relatively low specificity of *Sm*NDPKs to various nucleotides and deoxy nucleotides tested, similarly to what has been described for other NDPKs [8].

## 5- DISCUSSION

Besides the huge structural information, the catalytic mechanism of NDPKs occurs through a very complex, but well-determined sequence of events that are well described and studied [6, 8, 44]. As previously characterized, the NTP phosphate donor binds in the catalytic pocket, located on the surface of each subunit of the hexamer. The NTP concentration is the main factor to determine which donor will be bound (since there is abundant ATP concentration in the cells, it is the most used NTP by NDPKs). In the next step, the catalytic histidine (H115 in *Schistosoma mansoni* NDPK determined based on sequence alignment) is phosphorylated by transferring the phosphate- $\gamma$  group (phosphate group furthest from the base), resulting in an intermediate state of the enzyme with the presence of a phosphohistidine. The phosphate group stabilization to form the phosphohistidine is aided by the action of serine S117, which helps to accommodate the phosphate group in the space left by the presence of G116. The concentration increases of a different NDP than that which is bound to the catalytic site displaces the equilibrium and makes the nucleotide leave the active site for the entry of a receptor nucleotide. The receptor NDP receives the phosphate group bound to phosphohistidine and leaves the site as a new NTP. When the *Sm*NDPK-apo and ADP structures were compared by superposition, no significant structural changes in active site were observed.

The binding assays reveal an ATP/GTP preference during the first step formation (dissociation constants in  $(3.10 \pm 0.02) \mu\text{M}$  and  $(3.30 \pm 0.07) \mu\text{M}$ , respectively), which could be explained by the blood availability in comparison with others triphosphate nucleotides. In addition, the sequential interaction using non-hydrolyzed nucleotide, ATP $\gamma$ S, showed that it has no preference for the second nucleotide (all the  $K_D$  are about  $10 \mu\text{M}$ ), indicating that the ATP/GTP are the major phosphate donors during the metabolic reaction. These hypotheses indicate the nucleotides pull is kept by the *Sm*NDPK, being highly active to be responsible for the diphosphate nucleotides conversion to triphosphates by ATP/GTP, obtained by feeding, as the  $\gamma$ -phosphate donor.

The kinetics assays also showed the *Sm*NDPK activity in function of  $\gamma$ -phosphate transfer from ATP to GDP, forming GTP and ADP. The  $K_M$  and  $k_{cat}$  values  $(36.3 \pm 1.6) \mu\text{M}$  and  $(0.68 \pm 0.01) \text{s}^{-1}$ , respectively, are 1000 fold higher in comparison to humans [43]

The GDP  $K_D$  for brown rats NDPK [45] is similar to that observed for *Sm*NDPK, while this value information for *Hs*NDPK is absent, preventing a comparison. Interestingly, the  $k_{cat}$  value is more than 300 fold smaller in comparison to all the previous results observed [46, 47].

A proteomic study has detected *Sm*NDPK in the vomitus of adult worms [40], thus suggesting a role in parasite digestion of human blood. The fact that we detected transcripts in the anterior esophagus of the parasite using WISH reinforces the idea that *Sm*NDPK might be in contact with incoming blood. A possible explanation is that extracellular ATP serves as a signal of cell distress that recruits cells involved in inflammatory responses [48]. Considering that ingested leukocytes will be under significant stress, the fact that *Sm*NDPK can convert the excess of extracellular ATP produced by such cells into other nucleotides might represent a mechanism to defuse such signaling while preserving overall level of triphosphate nucleotides for absorption and further use as energy source or metabolic components. The observed high affinity to ATP reinforces the notion that *Sm*NDPK presence in the digestive system should be related to the enzymatic breakdown of this molecule.

*Sm*NDPK is also present in a list of 463 detected in a proteomic study as exposed at the surface of recently transformed schistosomula. Considering that it is known that invading schistosomula will be met with inflammatory responses [49], proteins involved in nucleotide metabolism, such as *Sm*NDPK, could also play a role in diminishing extracellular ATP levels to avoid an exacerbated inflammatory response.

In addition, examination of previously RNA-Seq experiment measuring differential expression in adult worm gonads [39] showed *Sm*NDPK as upregulated in the ovary of paired females. In the present work, WISH using a probe for *Sm*NDPK resulted in a strongly visible signal in the gonads. We have recently identified *Sm*APRT in the ovary and vitellaria of female adult worms, where it might share with *Sm*NDPK a role in energy acquisition to support the intense egg production [50]. *Sm*NDPK, however, was also detected in the testis of male worms, suggesting a broad function related to gonads.

The *Sm*NDPK structure and kinetic activity presented here represent our latest effort to fully characterize the *S. mansoni* purine salvage pathway [50-63]. The association of *Sm*NDPK with processes related to host-parasite interaction and sexual



biology of the parasite makes it an interesting target for possible therapies, with further studies warranted to verify its potential.

## **6- Acknowledgments**

This work was funded by FAPESP, CNPq and Instituto de Física de São Carlos, Universidade de São Paulo. This work was supported by Grants 2012/14223-9 (HMP), 2012/10213-9 (JRT), 2012/23730-1 (VHBS), 2013/20715-4 (AEZ) from São Paulo Research Foundation (FAPESP) and CNPq 474402/2013-4 (HMP); 134013/2015-8 (AFF), 140636/2013-7 (VHBS) and MR/K018779/1 (LEB, JEN, RJO). Also, we would like to thank CAPES. We acknowledge Leticia Anderson and Sergio Verjovski-Almeida for providing adult *S. mansoni* worms to perform the WISH experiment.

## 7- References

- [1] R.L. Ratliff, R.H. Weaver, H.A. Lardy, S.A. Kuby, Nucleoside Triphosphate-Nucleoside Diphosphate Transphosphorylase (Nucleoside Diphosphokinase). I. Isolation of the Crystalline Enzyme from Brewers' Yeast, *J Biol Chem* 239 (1964) 301-9.
- [2] P. Berg, W.K. Joklik, Transphosphorylation between nucleoside polyphosphates, *Nature* 172(4387) (1953) 1008-9.
- [3] R.E. Parks Jr, R.P. Aganwal, 9 Nucleoside Diphosphokinases, in: D.B. Paul (Ed.), *The Enzymes*, Academic Press 1973, pp. 307-333.
- [4] J. Bourdais, R. Biondi, S. Sarfati, C. Guerreiro, I. Lascu, J. Janin, M. Veron, Cellular phosphorylation of anti-HIV nucleosides. Role of nucleoside diphosphate kinase, *J Biol Chem* 271(14) (1996) 7887-90.
- [5] S.A. Kuby, G. Fleming, T. Alber, D. Richardson, H. Takenaka, M. Hamada, Studies on yeast nucleoside triphosphate-nucleoside diphosphate transphosphorylase (nucleoside diphosphokinase). IV. Steady-state kinetic properties with thymidine nucleotides (including 3'-azido-3'-deoxythymidine analogues), *Enzyme* 45(1-2) (1991) 1-13.
- [6] C. Dumas, I. Lascu, S. Morera, P. Glaser, R. Fourme, V. Wallet, M.L. Lacombe, M. Veron, J. Janin, X-ray structure of nucleoside diphosphate kinase, *EMBO J* 11(9) (1992) 3203-8.
- [7] N. Mourad, R.E. Parks, Jr., Erythrocytic nucleoside diphosphokinase. II. Isolation and kinetics, *J Biol Chem* 241(2) (1966) 271-8.
- [8] P. Gonin, Y. Xu, L. Milon, S. Dabernat, M. Morr, R. Kumar, M.L. Lacombe, J. Janin, I. Lascu, Catalytic mechanism of nucleoside diphosphate kinase investigated using nucleotide analogues, viscosity effects, and X-ray crystallography, *Biochemistry* 38(22) (1999) 7265-72.
- [9] A. Mehta, S. Orchard, Nucleoside diphosphate kinase (NDPK, NM23, AWD): recent regulatory advances in endocytosis, metastasis, psoriasis, insulin release, fetal erythroid lineage and heart failure; translational medicine exemplified, *Mol Cell Biochem* 329(1-2) (2009) 3-15.
- [10] Y.F. Liu, A. Yang, W. Liu, C. Wang, M. Wang, L. Zhang, D. Wang, J.F. Dong, M. Li, NME2 reduces proliferation, migration and invasion of gastric cancer cells to limit metastasis, *PLoS One* 10(2) (2015) e0115968.
- [11] WORLD HEALTH ORGANIZATION, WHO - Schistosomiasis, 2017. <http://www.who.int/mediacentre/factsheets/fs115/en/>. (Accessed 02/2017 2017).
- [12] G.W. Crabtree, A.W. Senft, Pathways of nucleotide metabolism in schistosoma mansoni. V. Adenosine cleavage enzyme and effects of purine analogues on adenosine metabolism in vitro, *Biochem Pharmacol* 23(3) (1974) 649-60.
- [13] F.P. Miech, A.W. Senft, D.G. Senft, Pathways of nucleotide metabolism in Schistosoma mansoni--VI adenosine phosphorylase, *Biochem Pharmacol* 24(3) (1975) 407-11.
- [14] A.W. Senft, G.W. Crabtree, Pathways of nucleotide metabolism in Schistosoma mansoni--VII. Inhibition of adenine and guanine nucleotide synthesis by purine analogs in intact worms, *Biochem Pharmacol* 26(20) (1977) 1847-55.
- [15] A.W. Senft, G.W. Crabtree, Purine metabolism in the schistosomes: potential targets for chemotherapy, *Pharmacol Ther* 20(3) (1983) 341-56.
- [16] A.W. Senft, G.W. Crabtree, K.C. Agarwal, E.M. Scholar, R.P. Agarwal, R.E. Parks, Jr., Pathways of nucleotide metabolism in Schistosoma mansoni. 3.

- Identification of enzymes in cell-free extracts, *Biochem Pharmacol* 22(4) (1973) 449-58.
- [17] A.W. Senft, R.P. Miech, P.R. Brown, D.G. Senft, Purine metabolism in *Schistosoma mansoni*, *International journal for parasitology* 2(2) (1972) 249-60.
- [18] A.W. Senft, D.G. Senft, R.P. Miech, Pathways of nucleotide metabolism in *Schistosoma mansoni*. II. Disposition of adenosine by whole worms, *Biochem Pharmacol* 22(4) (1973) 437-47.
- [19] R.J. Stegman, A.W. Senft, P.R. Brown, R.E. Parks, Jr., Pathways of nucleotide metabolism in *Schistosoma mansoni*. IV. Incorporation of adenosine analogs in vitro, *Biochem Pharmacol* 22(4) (1973) 459-68.
- [20] H.F. Dovey, J.H. McKerrow, C.C. Wang, Purine salvage in *Schistosoma mansoni* schistosomules, *Molecular and biochemical parasitology* 11 (1984) 157-67.
- [21] W.E. Secor, D.G. Colley, *Schistosomiasis*, Springer Science + Business Media, Inc, Boston 2005.
- [22] N.S. Berrow, D. Alderton, S. Sainsbury, J. Nettleship, R. Assenberg, N. Rahman, D.I. Stuart, R.J. Owens, A versatile ligation-independent cloning method suitable for high-throughput expression screening applications, *Nucleic Acids Res* 35(6) (2007) e45.
- [23] M.J. Todd, J. Gomez, Enzyme kinetics determined using calorimetry: a general assay for enzyme activity?, *Anal Biochem* 296(2) (2001) 179-87.
- [24] N.A. Demarse, M.C. Killian, L.D. Hansen, C.F. Quinn, Determining enzyme kinetics via isothermal titration calorimetry, *Methods Mol Biol* 978 (2013) 21-30.
- [25] M.W. Freyer, E.A. Lewis, Isothermal titration calorimetry: experimental design, data analysis, and probing macromolecule/ligand binding and kinetic interactions, *Methods Cell Biol* 84 (2008) 79-113.
- [26] M.K. Transtrum, L.D. Hansen, C. Quinn, Enzyme kinetics determined by single-injection isothermal titration calorimetry, *Methods* 76 (2015) 194-200.
- [27] S.N. Olsen, E. Lumby, K. McFarland, K. Borch, P. Westh, Kinetics of enzymatic high-solid hydrolysis of lignocellulosic biomass studied by calorimetry, *Appl Biochem Biotechnol* 163(5) (2011) 626-35.
- [28] G. Winter, C.M. Lobley, S.M. Prince, Decision making in xia2, *Acta crystallographica. Section D, Biological crystallography* 69(Pt 7) (2013) 1260-73.
- [29] P.R. Evans, G.N. Murshudov, How good are my data and what is the resolution?, *Acta Crystallographica Section D-Biological Crystallography* 69 (2013) 1204-1214.
- [30] W. Kabsch, Xds, *Acta Crystallographica Section D-Biological Crystallography* 66 (2010) 125-132.
- [31] D.G. Waterman, G. Winter, R.J. Gildea, J.M. Parkhurst, A.S. Brewster, N.K. Sauter, G. Evans, Diffraction-geometry refinement in the DIALS framework, *Acta Crystallogr D Struct Biol* 72(Pt 4) (2016) 558-75.
- [32] A.J. McCoy, R.W. Grosse-Kunstleve, P.D. Adams, M.D. Winn, L.C. Storoni, R.J. Read, Phaser crystallographic software, *J Appl Crystallogr* 40(Pt 4) (2007) 658-674.
- [33] P.D. Adams, P.V. Afonine, G. Bunkoczi, V.B. Chen, I.W. Davis, N. Echols, J.J. Headd, L.W. Hung, G.J. Kapral, R.W. Grosse-Kunstleve, A.J. McCoy, N.W. Moriarty, R. Oeffner, R.J. Read, D.C. Richardson, J.S. Richardson, T.C. Terwilliger, P.H. Zwart, PHENIX: a comprehensive Python-based system for macromolecular structure solution, *Acta crystallographica. Section D, Biological crystallography* 66(Pt 2) (2010) 213-21.
- [34] P. Emsley, K. Cowtan, Coot: model-building tools for molecular graphics, *Acta Crystallogr D Biol Crystallogr* 60(Pt 12 Pt 1) (2004) 2126-32.

- [35] V.B. Chen, W.B. Arendall, 3rd, J.J. Headd, D.A. Keedy, R.M. Immormino, G.J. Kapral, L.W. Murray, J.S. Richardson, D.C. Richardson, MolProbity: all-atom structure validation for macromolecular crystallography, *Acta crystallographica. Section D, Biological crystallography* 66(Pt 1) (2010) 12-21.
- [36] A.A. Cogswell, J.J. Collins, P.A. Newmark, D.L. Williams, Whole mount in situ hybridization methodology for *Schistosoma mansoni*, *Molecular and biochemical parasitology* 178(1-2) (2011) 46-50.
- [37] G.P. Dillon, J.C. Illes, H.V. Isaacs, R.A. Wilson, Patterns of gene expression in schistosomes: localization by whole mount in situ hybridization, *Parasitology* 134(11) (2007).
- [38] F.J. Logan-Klumpler, N. De Silva, U. Boehme, M.B. Rogers, G. Velarde, J.A. McQuillan, T. Carver, M. Aslett, C. Olsen, S. Subramanian, I. Phan, C. Farris, S. Mitra, G. Ramasamy, H. Wang, A. Tivey, A. Jackson, R. Houston, J. Parkhill, M. Holden, O.S. Harb, B.P. Brunk, P.J. Myler, D. Roos, M. Carrington, D.F. Smith, C. Hertz-Fowler, M. Berriman, GeneDB--an annotation database for pathogens, *Nucleic Acids Res* 40(Database issue) (2012) D98-108.
- [39] Z. Lu, F. Sessler, N. Holroyd, S. Hahnel, T. Quack, M. Berriman, C.G. Greveling, Schistosome sex matters: a deep view into gonad-specific and pairing-dependent transcriptomes reveals a complex gender interplay, *Sci Rep* 6 (2016) 31150.
- [40] S.L. Hall, S. Braschi, M. Truscott, W. Mathieson, I.M. Cesari, R.A. Wilson, Insights into blood feeding by schistosomes from a proteomic analysis of worm vomitus, *Mol Biochem Parasit* 179(1) (2011) 18-29.
- [41] J.M. Berg, J.L. Tymoczko, L. Stryer, *Biochemistry*, 5th edition, W H Freeman, New York, 2002.
- [42] M. Brodbeck, A. Rohling, W. Wohlleben, C.J. Thompson, U. Susstrunk, Nucleoside-diphosphate kinase from *Streptomyces coelicolor*, *Eur J Biochem* 239(1) (1996) 208-13.
- [43] S.C. Lam, M.A. Packham, Isolation and kinetic studies of nucleoside diphosphokinase from human platelets and effects of cAMP phosphodiesterase inhibitors, *Biochem Pharmacol* 35(24) (1986) 4449-55.
- [44] A. Lecroisey, I. Lascu, A. Bominaar, M. Veron, M. Delepierre, Phosphorylation mechanism of nucleoside diphosphate kinase: <sup>31</sup>P-nuclear magnetic resonance studies, *Biochemistry* 34(38) (1995) 12445-50.
- [45] N. Kimura, N. Shimada, Membrane-associated nucleoside diphosphate kinase from rat liver. Purification, characterization, and comparison with cytosolic enzyme, *J Biol Chem* 263(10) (1988) 4647-53.
- [46] M. Johansson, J. Hammargren, E. Uppsäll, A. MacKenzie, C. Knorpp, The activities of nucleoside diphosphate kinase and adenylate kinase are influenced by their interaction, *Plant Science* 174(2) (2008) 192-199.
- [47] F. Georgescauld, L. Moynie, J. Habersetzer, L. Cervoni, I. Mocan, T. Borza, P. Harris, A. Dautant, I. Lascu, Intersubunit ionic interactions stabilize the nucleoside diphosphate kinase of *Mycobacterium tuberculosis*, *PLoS One* 8(3) (2013) e57867.
- [48] F. Di Virgilio, M. Vuerich, Purinergic signaling in the immune system, *Auton Neurosci* 191 (2015) 117-23.
- [49] A.P. Mountford, F. Trottein, Schistosomes in the skin: a balance between immune priming and regulation, *Trends Parasitol* 20(5) (2004) 221-6.
- [50] A.E. Zeraik, V.H. Balasco Serrao, L. Romanello, J.R. Torini, A. Cassago, R. DeMarco, H.D. Pereira, *Schistosoma mansoni* displays an adenine

phosphoribosyltransferase preferentially expressed in mature female gonads and vitelaria, *Molecular and biochemical parasitology* 214 (2017) 82-86.

[51] M.S. Castilho, M.P. Postigo, H.M. Pereira, G. Oliva, A.D. Andricopulo, Structural basis for selective inhibition of purine nucleoside phosphorylase from *Schistosoma mansoni*: kinetic and structural studies, *Bioorganic & medicinal chemistry* 18(4) (2010) 1421-7.

[52] H. D'Muniz Pereira, G. Oliva, R.C. Garratt, Purine nucleoside phosphorylase from *Schistosoma mansoni* in complex with ribose-1-phosphate, *J Synchrotron Radiat* 18(1) (2011) 62-5.

[53] A. Marques Ide, L. Romanello, R. DeMarco, H.D. Pereira, Structural and kinetic studies of *Schistosoma mansoni* adenylate kinases, *Molecular and biochemical parasitology* 185(2) (2012) 157-60.

[54] H.M. Pereira, V. Berdini, M.R. Ferri, A. Cleasby, R.C. Garratt, Crystal structure of *Schistosoma* purine nucleoside phosphorylase complexed with a novel monocyclic inhibitor, *Acta tropica* 114(2) (2010) 97-102.

[55] H.M. Pereira, A. Cleasby, S.S. Pena, G.G. Franco, R.C. Garratt, Cloning, expression and preliminary crystallographic studies of the potential drug target purine nucleoside phosphorylase from *Schistosoma mansoni*, *Acta crystallographica. Section D, Biological crystallography* 59(Pt 6) (2003) 1096-9.

[56] H.M. Pereira, M.M. Rezende, M.S. Castilho, G. Oliva, R.C. Garratt, Adenosine binding to low-molecular-weight purine nucleoside phosphorylase: the structural basis for recognition based on its complex with the enzyme from *Schistosoma mansoni*, *Acta crystallographica. Section D, Biological crystallography* 66(Pt 1) (2010) 73-9.

[57] M.P. Postigo, R. Krogh, M.F. Terni, H.M. Pereira, G. Oliva, M.S. Castilho, A.D. Andricopulo, Enzyme Kinetics, Structural Analysis and Molecular Modeling Studies on a Series of *Schistosoma mansoni* PNP Inhibitors, *Journal of the Brazilian Chemical Society* 22(3) (2011) 583-591.

[58] L. Romanello, J.F. Bachega, A. Cassago, J. Brandao-Neto, R. DeMarco, R.C. Garratt, H.D. Pereira, Adenosine kinase from *Schistosoma mansoni*: structural basis for the differential incorporation of nucleoside analogues, *Acta crystallographica. Section D, Biological crystallography* 69(Pt 1) (2013) 126-36.

[59] L. Romanello, V.H.B. Serrao, J.R. Torini, L.E. Bird, J.E. Nettleship, H. Rada, Y. Reddivari, R.J. Owens, R. DeMarco, J. Brandao-Neto, H.D. Pereira, Structural and kinetic analysis of *Schistosoma mansoni* Adenylosuccinate Lyase (SmADSL), *Molecular and biochemical parasitology* 214 (2017) 27-35.

[60] J.R. Torini, J. Brandao-Neto, R. DeMarco, H.D. Pereira, Crystal Structure of *Schistosoma mansoni* Adenosine Phosphorylase/5'-Methylthioadenosine Phosphorylase and Its Importance on Adenosine Salvage Pathway, *PLoS neglected tropical diseases* 10(12) (2016) e0005178.

[61] V.H.B. Serrao, H.D. Pereira, J.R.T. de Souza, L. Romanello, *Schistosoma mansoni* purine and pyrimidine biosynthesis: structures and kinetic experiments in the search for the best therapeutic target, *Current pharmaceutical design* (2017).

[62] H.D. Pereira, G.R. Franco, A. Cleasby, R.C. Garratt, Structures for the potential drug target purine nucleoside phosphorylase from *Schistosoma mansoni* causal agent of schistosomiasis, *Journal of molecular biology* 353(3) (2005) 584-99.

[63] J.R. Torini, L. Romanello, F.A.H. Batista, V.H.B. Serrao, M. Faheem, A.E. Zeraik, L. Bird, J. Nettleship, Y. Reddivari, R. Owens, R. DeMarco, J.C. Borges, J. Brandao-Neto, H.D. Pereira, The molecular structure of *Schistosoma mansoni* PNP isoform 2 provides insights into the nucleoside selectivity of PNPs, *PloS one* 13(9) (2018) e0203532.

### Legends:

Table 1. Kinetics parameters from *Sm*NDPK during the binding and enzymatic assays.

Table2. Data collection, processing and refinement statistics of *Sm*NDPK.

Figure 1. Sequence alignment showing the secondary structure elements comparing *Sm*NDPK with both human homologues (*Hs*NDPK-A and *Hs*NDPK-B) generated by the Esprint server.

Figure 2. Localization of NDPK transcripts by whole mount *in situ* hybridization in adult *S. mansoni* worms. (A) Female adult worm showing strong labeling in the entire ovary (A - upper arrow) and also staining in the vitellaria (lower arrow). (B) Part of the female worm body exposed to hybridization solution containing antisense *Sm*NDPK riboprobe; strong staining in the vitellaria (arrowed) is noticeable. (C) Male adult worms presenting labeling in the testis (arrow) and anterior esophagus region (arrowhead). (D) Control female and male worms incubated with sense RNA strand.

Figure 3. The binding assays comparing of *Sm*NDPK. Multiple injection by ITC showing the binding profile for ATP, GTP, CTP, TTP, UTP and ATP $\gamma$ S (A to F), respectively, also as negative control: Bovine Serum Albumin (BSA) interacting with ATP and ATP $\gamma$ S (G and H) was used as negative control. The kinetics parameters are showed in Table 1.

Figure 4. The binding assays in presence of non-hydrolysable ATP $\gamma$ S. Multiple injection by ITC showing the binding profile for ADP, GDP, CDP, TDP and UDP (A to E), respectively. The kinetics parameters are showed in Table 1.

Figure 5. *Sm*NDPK structure. (A) The macromolecular assembly observed in the asymmetric unit revealing-revealed the canonical hexamer oligomerization, or a dimer of trimers. (B) The monomer molecule-topology shows a canonical Nucleoside diphosphate kinase-like domain (CATH 3.30.70.141), or an alpha-beta 2-layers sandwich.

Figure 6. Analysis of the *Sm*NDPK.ADP complex. (A) Composit omit map countered at 1.7 sigma of ADP molecules in the *Sm*NDPK active site. (B) Active site of *Sm*NDPK with bounded-bound ADP. (B) Composit omit map countored at 1.7 sigma of ADP molecules in the NDPK active site. (C) The ligand-plot schematic generated by the Lidia software. Highlighting the important residues responsible for the “ping-pong” catalysis [3], as the H115, not involved directly into the binding, but being crucial for the kinetic effect in this enzyme class.

**Table 1.**

|                                |                                | <u>Binding assays</u>                |   | HMDB                            | <u>Kinetics assays</u>                               |                                      |
|--------------------------------|--------------------------------|--------------------------------------|---|---------------------------------|--|--------------------------------------|
|                                |                                | $K_D^{\text{avg}}$ ( $\mu\text{M}$ ) | $\Delta H_{\text{app}}^{\text{avg}}$ (kcal/mol) | concentration ( $\mu\text{M}$ ) | $K_M$ ( $\mu\text{M}$ )                              | $k_{\text{cat}}$ ( $\text{s}^{-1}$ ) |
|                                | <b>ATP</b>                     | $3.10 \pm 0.02$                      | $+(3.3 \pm 0.3)$                                | $> 1300$                        | -  | -                                    |
|                                | <b>GTP</b>                     | $3.30 \pm 0.07$                      | $-(3.0 \pm 0.7)$                                | $56.0 \pm 7.0$                  | -  | -                                    |
|                                | <b>CTP</b>                     | -                                    | -   | 28.0                            | -  | -                                    |
|                                | <b>TTP</b>                     | $10.0 \pm 1.6$                       | $-(2.3 \pm 0.1)$                                | -                               | -  | -                                    |
|                                | <b>UTP</b>                     | $9.9 \pm 1.3$                        | $-(9.8 \pm 5.1)$                                | -                               | -  | -                                    |
|                                | <b>ATP<math>\gamma</math>S</b> | $7.25 \pm 0.42$                      | $-(3.9 \pm 0.8)$                                | -                               | -  | -                                    |
|                                | <b>ADP</b>                     | $1.45 \pm 0.06$                      | $-(1.7 \pm 0.1)$                                | $160.0 \pm 14.0$                | $\Delta H_{\text{ATP/GDP}} = + 2.0 \text{ kcal/mol}$ |                                      |
|                                | <b>GDP</b>                     | $9.99 \pm 0.05$                      | $-(1.4 \pm 0.1)$                                | $15.0 \pm 2.0$                  | $36.3 \pm 1.6$                                       | $0.68 \pm 0.01$                      |
| <b>ATP<math>\gamma</math>S</b> | <b>CDP</b>                     | $10 \pm 5$                           | $-(9.6 \pm 2)$                                  | $36.0 \pm 12.0$                 | -  | -                                    |
|                                | <b>TDP</b>                     | $9.9 \pm 0.4$                        | $-(14.4 \pm 0.4)$                               | -                               | -  | -                                    |
|                                | <b>UDP</b>                     | $9.4 \pm 0.4$                        | $-(17.3 \pm 2.7)$                               | $41.0 \pm 12.0$                 | -  | -                                    |



**Table 2.**

|                                    | <i>SmNDPK-apo-C<sub>2</sub></i> | <i>SmNDPK-apo P6<sub>3</sub>22</i> | <i>SmNDPK-ADP</i>          |
|------------------------------------|---------------------------------|------------------------------------|----------------------------|
| Detector                           | Pilatus 2M                      | Pilatus 2M                         | Pilatus 2M                 |
| Cell parameters (Å)                | 211.76;                         | 71.59; 71.59; 219.44               | 71.45; 71.45;              |
| a; b;c                             | 82.27; 122.37                   | 90; 90; 120                        | 219.34                     |
|                                    | 90; 104.89; 90                  |                                    | 90; 90; 120                |
| Space Group                        | C2                              | P6 <sub>3</sub> 22                 | P6 <sub>3</sub> 22         |
| Resolution (Å)                     | 59.1- 1.74<br>(1.79-1.74)       | 47.30 - 1.90 (1.95-<br>1.90)       | 61.8- 2.11<br>(2.16 -2.11) |
| X-ray Source                       | I04-1                           | I04-1                              | I04-1                      |
| $\lambda$ (Å)                      | 0.92                            | 0.92                               | 0.92                       |
| Multiplicity                       | 3.4 (3.3)                       | 9.6 (10.0)                         | 18.9 (19.6)                |
| R <sub>merge</sub> (%)             | 7.0 (70.4)                      | 10.4 (70.4)                        | 8.5 (71.0)                 |
| R <sub>pim</sub> (%)               | 4.4 (45.9)                      | 3.5 (23.1)                         | 2.0 (16.4)                 |
| CC(1/2)                            | 0.997 (0.6440)                  | 0.998 (0.846)                      | 1.0 (0.936)                |
| Completeness (%)                   | 98.4 (98.3)                     | 99.6 (98.6 - 99.5)                 | 100 (99.4 -<br>100 )       |
| Reflections                        | 695442<br>(49438)               | 261734 (19271)                     | 379170<br>(28386)          |
| Unique Reflections                 | 204192<br>(15018)               | 27155 (1934)                       | 20075 (1450)               |
| <i>I</i> / $\sigma$                | 11.2 (1.9)                      | 15.3 (3.6)                         | 27.7 (5.1)                 |
| Reflections used for<br>Refinement | 204169                          | 27125                              | 20023                      |
| R(%)**                             | 16.44                           | 16.21                              | 16.82                      |
| R <sub>free</sub> (%)**            | 19.09                           | 20.77                              | 19.87                      |
| N° of protein atoms                | 14205                           | 2372                               | 2353                       |
| N° of ligant atoms                 | 0                               | 0                                  | 54                         |
| B (Å <sup>2</sup> )                | 21.60                           | 23.07                              | 36.28                      |
| B (Å <sup>2</sup> ) ADP            | -                               | -                                  | 77.27                      |
| Coordinate Error (ML<br>based) (Å) | 0.20                            | 0.18                               | 0.19                       |
| Phase error (°)                    | 19.29                           | 19.46                              | 19.04                      |
| <i>Ramachandran Plot</i>           |                                 |                                    |                            |
| Favored (%)                        | 97.29                           | 97.64                              | 97.97                      |
| Allowed (%)                        | 1.97                            | 1.68                               | 1.36                       |
| Outliers (%)                       | 0.73                            | 0.67                               | 0.68                       |
| All-atom Clashscore                | 2.33                            | 1.69                               | 3.15                       |
| <i>RMSD from ideal geometry</i>    |                                 |                                    |                            |
| r.m.s. bond lengths (Å)            | 0.005                           | 0.011                              | 0.007                      |
| r.m.s. bond angles (°)             | 0.716                           | 1.023                              | 0.962                      |

Figure 1

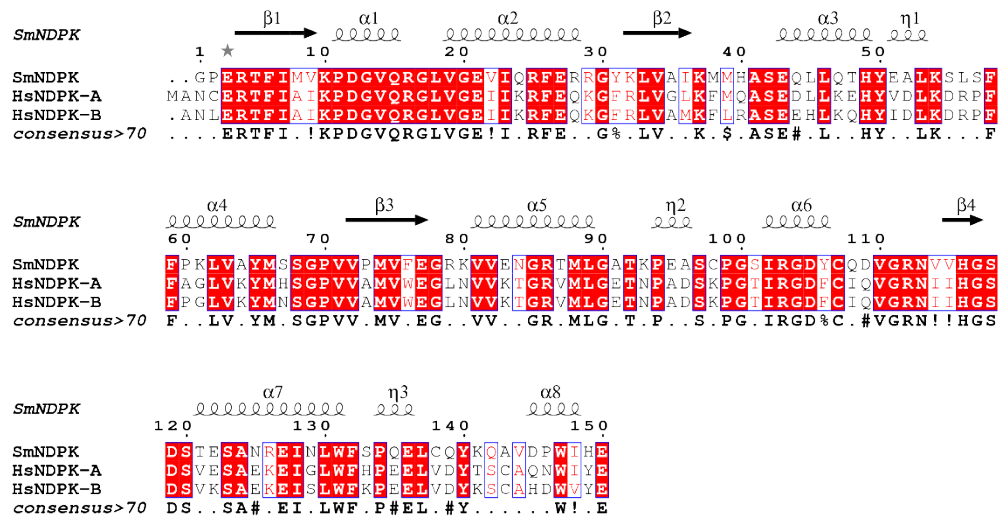
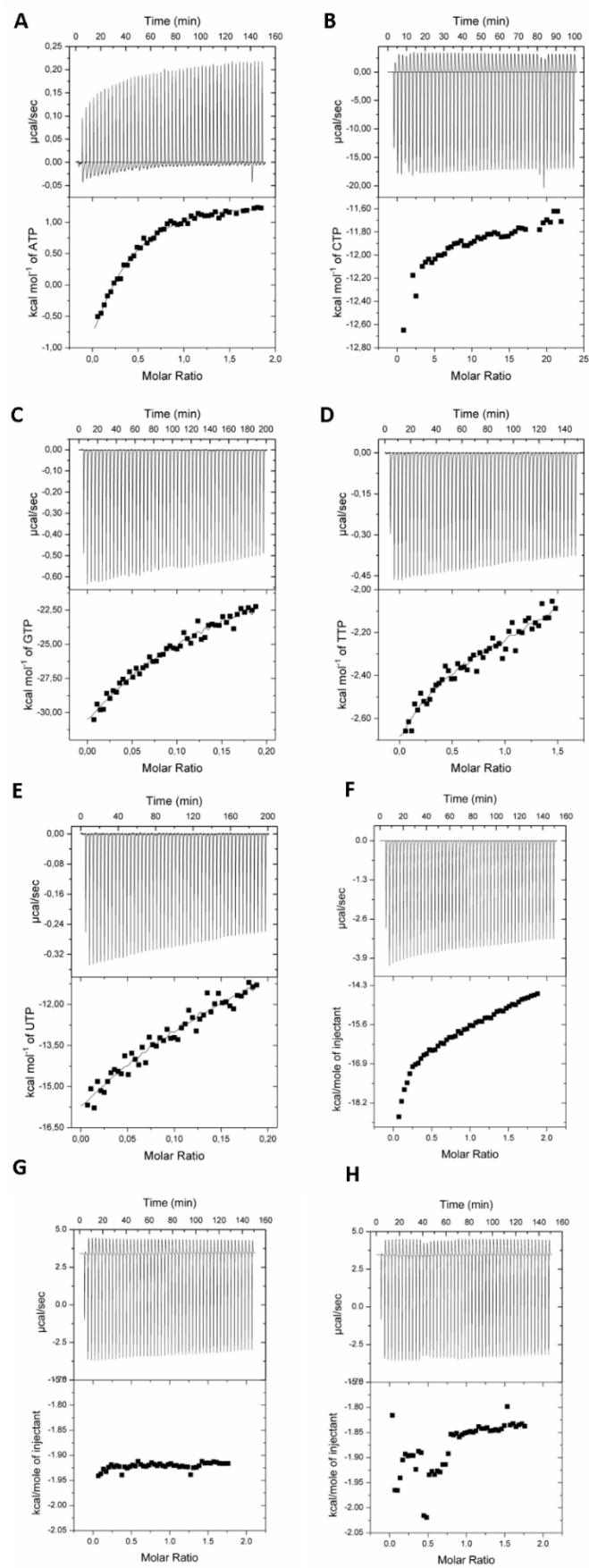


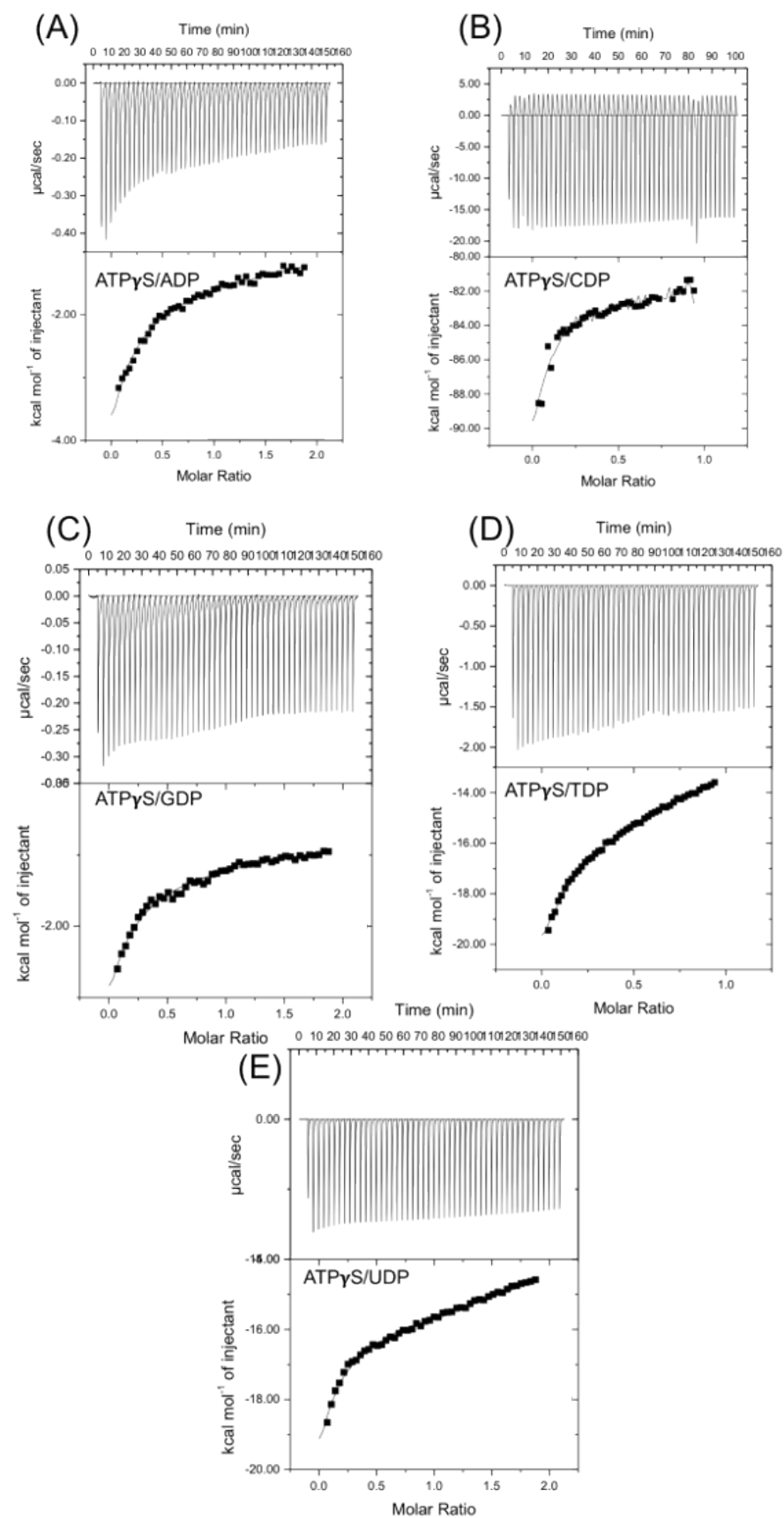
Figure 2



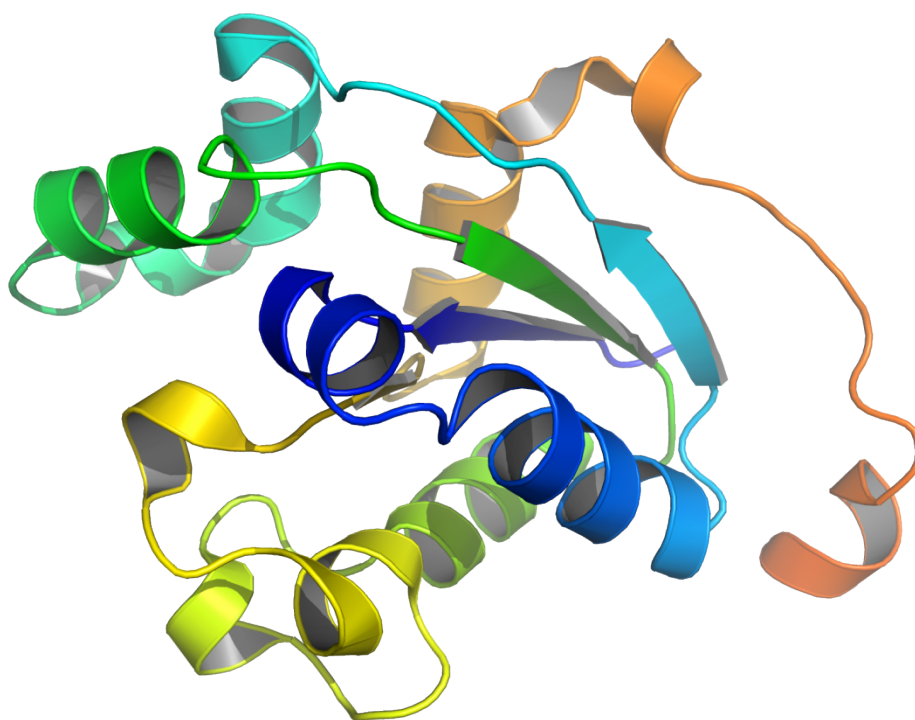
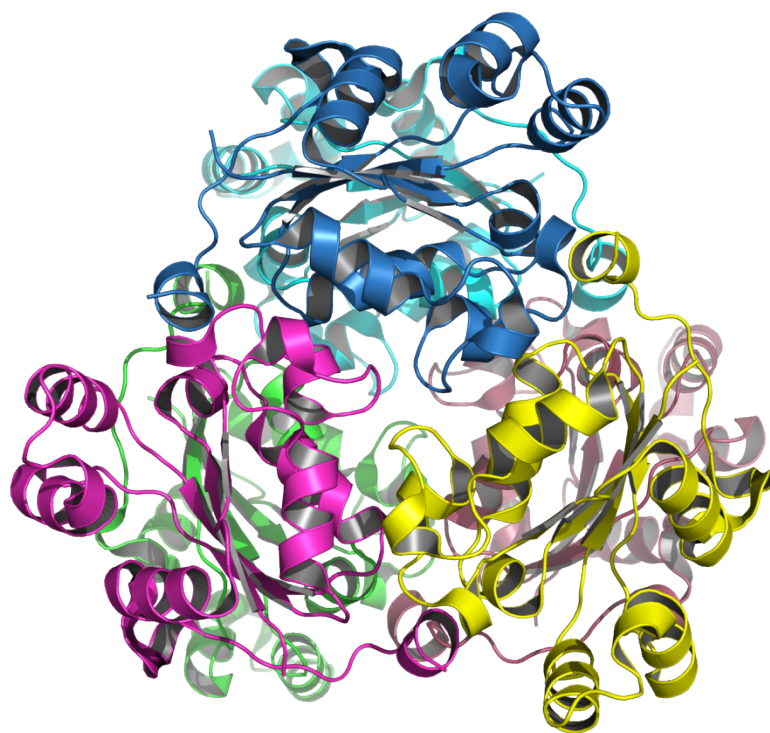
### **Figure 3**



**Figure 4**



**Figure 5**





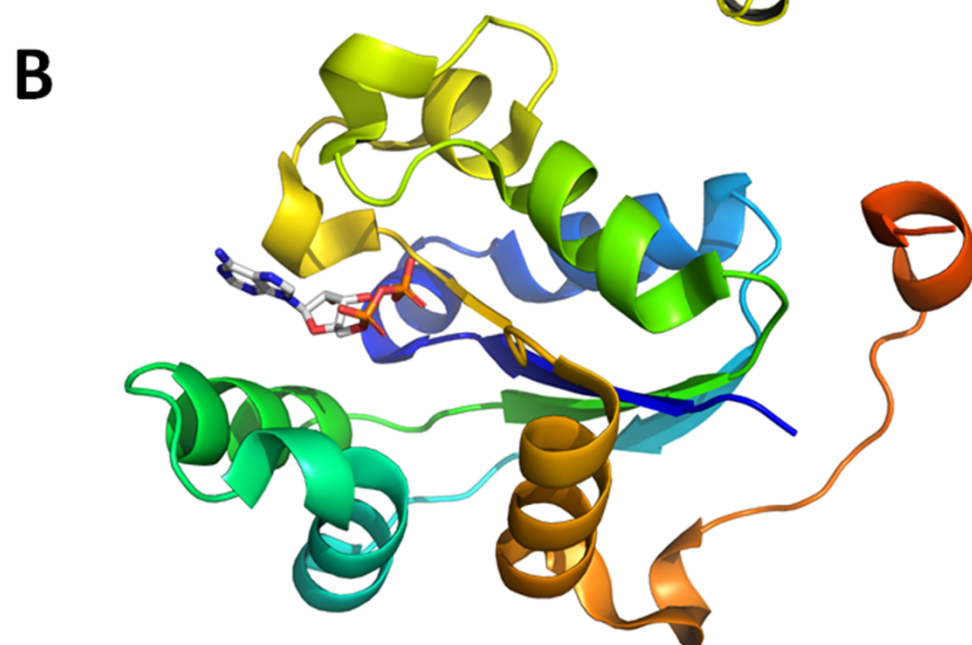
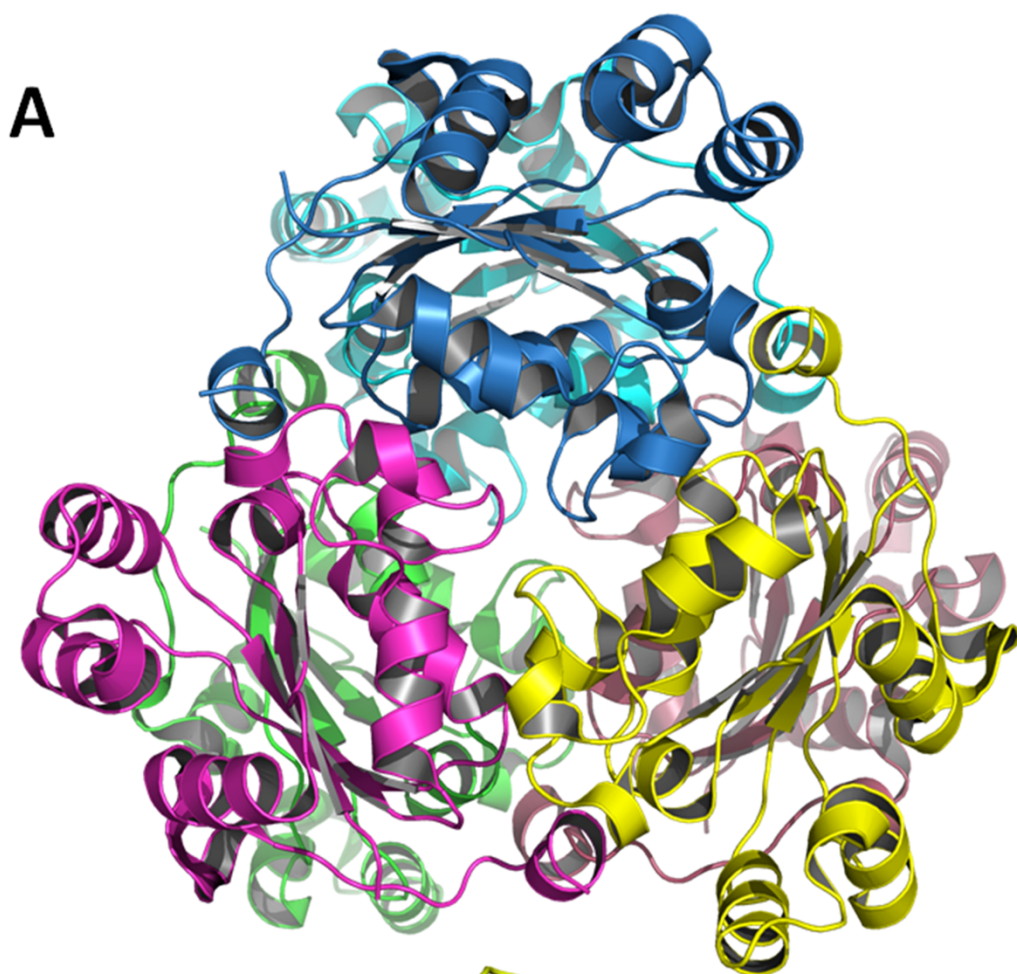




**Figure 6**

